Model Updating Strategy for Structures with Localised Nonlinearities using Frequency Response Measurements

Xing Wang[a], Thomas L. Hill[a], Simon A. Neild[a],

Alexander D. Shaw[b], Hamed Haddad Khodaparast[b], Michael I. Friswell[b]

[a]Department of Mechanical Engineering, University of Bristol, Bristol BS8 1TR, United Kingdom

[b]College of Engineering, Swansea University, Swansea SA1 8EN, United Kingdom

Abstract

This paper proposes a model updating strategy for localised nonlinear structures. It utilises an initial finite-element (FE) model of the structure and primary harmonic response data taken from low and high amplitude excitations. The underlying linear part of the FE model is first updated using low-amplitude test data with established techniques. Then, using this linear FE model, the nonlinear elements are localised, characterised, and quantified with primary harmonic response data measured under stepped-sine or swept-sine excitations. Finally, the resulting model is validated by comparing the analytical predictions with both the measured responses used in the updating and with additional test data. The proposed strategy is applied to a clamped beam with a nonlinear mechanism and good agreements between the analytical predictions and measured responses are achieved. Discussions on issues of damping estimation and dealing with data from amplitude-varying force input in the updating process are also provided.

Keywords: nonlinear model updating, localised nonlinearities, frequency response measurement

1. Introduction

Using linear finite-element (FE) models as prototypes to predict structural dynamic behaviours in the design stage is widely accepted in the engineering industry to reduce cost and time. These mathematical models are routinely updated by relaxing weak assumptions or modifying inaccurate parameters after vibration testing campaigns [1,2] to ensure high reliability for load analysis. In practice, many structures are unlikely to behave perfectly linearly during these tests, especially when they respond at large amplitudes. Currently it is common to neglect such nonlinearities as they have marginal effects. However, with the drive towards more efficient and flexible structures, nonlinear dynamic behaviour is inevitably becoming more common. For such structures, linear models no longer achieve high-fidelity predictions and may, in some instances, fail to capture critical dynamic behaviours.

An example of this in aerospace systems is the Cassini Spacecraft, where the longitudinal modal frequency of its payload, the Huygens probe, decreased as forcing level increased. This frequency reduction introduced coupling with the frequency band of high-energy excitation from the launch vehicle and resulted in 50% overload compared to its design requirements [3]. Kerschen *et al.* [4-6] also observed strong nonlinear behaviours of a wheel elastomer mounting system (WEMS) device during the Smallsat ground test campaign. The piecewise linear WEMS device in the satellite exhibited dynamic behaviours such as jumps and modal interactions that cannot be described using linear models. Göge *et al.* investigated typical nonlinear phenomena during ground vibration test campaigns on a large aircraft, and demonstrated multiple types of amplitude and/or frequency dependent behaviours [7]. Such nonlinear behaviours may also occur at interfaces when assembling individual sub-components, for example, bilinear stiffness at engine flange joints [8] or wing-pylon joints [9,10]. Along with nonlinearities that are intrinsic to a structure, engineers also intentionally design nonlinear mechanisms to achieve better performance. Examples include employing a nonlinear energy sink to suppress aeroelastic instability [11,12], introducing a nonlinear hinge between wing tips and the main

airframe to alleviate gust loads [13], and adding a nonlinear secondary spring to improve the vibration attenuation efficiency of a isolator [14]. These nonlinear mechanisms are typically local such that the number of nonlinear elements is far fewer than the total number of degrees of freedom (DOFs) in the structure; however, they can still result in significant nonlinear behaviours in the global dynamics [11-15].

In practical applications, nonlinear elements are often quite complex to model and accurate parameters are difficult to obtain directly. Thus, tremendous efforts have been devoted to identifying nonlinear elements based on the measured responses of an assembled structure. Kerschen [16] proposed a general nonlinear identification procedure consisting of three main steps (i.e., detection, characterisation and parameter estimation), where the characterisation step relied on the time domain restoring force surface (RFS) method [5] and the parameter estimation step utilises the conditioned reverse path (CRP) method [17] based on random response data. Two comprehensive reviews, including recent developments in this procedure, are documented in references [18] and [19]. Ewins *et al.* [20,21] proposed a 'Modal Test +' procedure to extend the established linear modal testing techniques for structures with discrete nonlinearities, which also relied on the restoring force surface method and the reverse path method [22] during characterisation and quantification steps, respectively. Recently, the nonlinear normal mode (NNM) based updating strategy [23-26] using measured time series has been presented and applied to the ECL benchmark beam [25] as well as the IMAC XXXII Round Robin benchmark system [26]. Currently, this strategy requires knowledge of the locations and types of nonlinearity present in the structure.

A nonlinear model updating strategy should also verify the updated model and minimise any discrepancy between the predictions and the measured responses [8,21,23-26]. To do this, residuals between measured responses and analytical predictions, based on the identified nonlinear model under the same input, must be extracted and then minimised. While broadband random excitation data, such as that used in the reverse path method, might be used for

this, it does raise some issues for large aerospace structures. Firstly, numerical simulations of a nonlinear model under random excitations with a given spectrum generally require time integration schemes. This can be computationally very expensive for a large-scale model during the multiple parameter iterations, as is often the case during updating. Secondly, the aerospace industry typically implements slow swept-sine or stepped-sine excitations to identify structural modal parameters, such as the standard and mandatory procedures adopted by NASA [3], ESA [27] and Airbus [28,29] during ground vibration test campaigns. It would be advantageous for the updating data to be obtained using similar tests for the sake of integration into existing testing practice. Thirdly, and most importantly, the demand to excite the structural modes with sufficient energy is crucial for large-scale aerospace structures. For example, an aircraft should be driven as close as possible to its operational energy levels during ground vibration test campaigns, in order to generate high-quality data to update its FE model or as evidence for the certification process [27,29]. For these applications, random excitation may not be able to excite the structure to sufficiently high amplitudes under actuating limits of current testing equipment [29].

To tackle these challenges, this paper presents a novel model updating strategy for structures with localised nonlinearities. The steps in the nonlinear identification process and numerical simulations are based on the primary harmonic frequency responses that can be obtained using current testing techniques in the aerospace industry; i.e. using stepped-sine or slow swept-sine excitations. It establishes two kinds of residuals to describe the test/analysis discrepancies and avoids computationally expensive time integration schemes by using a direct frequency domain residual minimisation process; this allows rapid iterations to refine the nonlinear FE models and improves the efficiency of updating.

The updating strategy comprises of three main processes: (1) structural testing to obtain the data; (2) linear model updating to construct an underlying linear FE model; (3) nonlinear model updating to localise the nonlinear elements,

characterise them, quantify their parameters and then validate the resulting model. These steps are described in detail and demonstrated by using experimental data to update a FE model of a clamped beam with a nonlinear mechanism connected near the tip in section 3 after the model formulation and residual definition given in section 2. The resulting model is then assessed using independent experimental data not used in the updating. Following this, Section 4 discusses the issues regarding the estimation of damping and dealing with amplitude-varying force input data in updating. Conclusions are drawn in section 5.

2. Equations and frequency domain residuals

In this section, the form of the equations of motion and the residuals between measured data and predicted responses will be introduced before the updating strategy is proposed in the next section.

2.1. Dynamic equation with location matrix

The dynamic equation of an *N*-DOF structure with γ inter-connected and/or grounded nonlinear elements can be expressed in a general form as

$$\mathbf{M}\ddot{\boldsymbol{x}} + \mathbf{C}\dot{\boldsymbol{x}} + \mathbf{K}\boldsymbol{x} + \boldsymbol{f}^*\left(\boldsymbol{x}, \dot{\boldsymbol{x}}\right) = \boldsymbol{p}\left(t\right), \tag{1}$$

where $\mathbf{M}$, $\mathbf{C}$, $\mathbf{K} \in \mathbb{R}^{N\times N}$ denote the mass, damping and stiffness matrices, respectively. $\boldsymbol{x}$, $\dot{\boldsymbol{x}}$, $\ddot{\boldsymbol{x}} \in \mathbb{R}^{N\times 1}$ denote the displacement, velocity and acceleration vectors described with physical coordinates, respectively. The vector $\boldsymbol{f}^*\left(\boldsymbol{x}, \dot{\boldsymbol{x}}\right) \in \mathbb{R}^{N\times 1}$ denotes the nonlinear force and vector $\boldsymbol{p}\left(t\right) \in \mathbb{R}^{N\times 1}$ is the external excitation force.

For localised nonlinear structures, the number of independent nonlinear elements is far fewer than the number of DOFs of the structure, i.e. $\gamma << N$. A unique feature of the localised nonlinear model having this characteristic is that the nonlinear force vector, $\boldsymbol{f}^*\left(\boldsymbol{x}, \dot{\boldsymbol{x}}\right)$, is sparsely populated with independent nonlinear forces [15,20]. Note that a well-conditioned identification procedure can be formulated by separating the nonlinear force vector and the underlying

linear system from a multiple-degree-of-freedom (MDOF) nonlinear structure [17,22]. Here, the conditioning problem during the identification procedure will be further improved by decoupling the nonlinear force vector with its non-zero values (scalar nonlinear forces) and their corresponding locations utilising its sparse nature. The dynamic equation incorporating the location matrix of the nonlinear elements will be defined first, for the case where measurements are spatially incomplete and the locations of the nonlinearities are not known. Following this, the equation and output residuals are proposed based on the resulting equation.

The kth localised nonlinear element either acts between DOFs i_k and j_k with the force generated by the element being a function of the relative motion between coordinates $x_{i_k} - x_{j_k}$ (inter-connected element) or acts at a DOF i_k, which we denote $i_k = j_k$, with a force based on the absolute motion of coordinate x_{i_k} (grounded element). We can describe the relative motion across the kth nonlinear element, r_k, with physical coordinates according to its connectivity [30], as

$$r_k = \begin{cases} x_{i_k} - x_{j_k}, & if \quad i_k \neq j_k \\ x_{i_k}, & if \quad i_k = j_k \end{cases}, \quad k = 1, 2, \ldots \gamma. \tag{2}$$

Alternatively, r_k can be written as

$$r_k = \boldsymbol{l}_k^{\mathrm{T}} \boldsymbol{x}, \text{ with: } \boldsymbol{l}_k = \begin{cases} \begin{bmatrix} 0 & 0 & \cdots & 0 & \underset{i_k}{1} & \underset{j_k}{-1} & \cdots & 0 \end{bmatrix}^{\mathrm{T}}, & \text{if} \quad i_k \neq j_k \\ \begin{bmatrix} 0 & 0 & \cdots & 0 & \underset{i_k}{1} & 0 & \cdots & 0 \end{bmatrix}^{\mathrm{T}}, & \text{if} \quad i_k = j_k \end{cases}, \; k = 1, 2, \ldots \gamma, \tag{3}$$

where $\boldsymbol{l}_k \in \mathbb{R}^{N \times 1}$ is the location vector for kth nonlinear element.

Defining the force generated by the kth discrete nonlinear element as $f_{\mathrm{nl},k}\left(r_k, \dot{r}_k\right)$, the nonlinear force vector in Eq. (1) may be written as

$$\boldsymbol{f}^*\left(\boldsymbol{x}, \dot{\boldsymbol{x}}\right) = \sum_{k=1}^{\gamma} \boldsymbol{l}_k f_{\mathrm{nl},k}\left(r_k, \dot{r}_k\right), \tag{4}$$

where $\boldsymbol{l}_k$ distributes the scalar force of the kth discrete nonlinear element to global physical coordinates, r_k and $\dot{r}_k$ denote the displacement and velocity of kth nonlinear element, respectively.

Defining a location matrix $\mathbf{L} \in \mathbb{R}^{N\times\gamma}$, which distributes the nonlinear forces to the correct degrees of freedom, and its transpose indicates the connectivity of relative motion, as

$$\mathbf{L}=\begin{bmatrix} \boldsymbol{l}_1 & \boldsymbol{l}_2 & \dots & \boldsymbol{l}_\gamma \end{bmatrix}, \tag{5}$$

and grouping the motion of nonlinear elements in a vector $\boldsymbol{r} \in \mathbb{R}^{\gamma\times 1}$ gives

$$\boldsymbol{r}=\left\{r_1, r_2, \cdots, r_\gamma\right\}^{\mathrm{T}}. \tag{6}$$

We can write, using Eqs. (4)-(6), that

$$\boldsymbol{f}^{*}\left(\boldsymbol{x}, \dot{\boldsymbol{x}}\right)=\mathbf{L}\boldsymbol{f}_{\mathrm{nl}}\left(\boldsymbol{r}, \dot{\boldsymbol{r}}\right), \quad \text{with: } \boldsymbol{r}=\mathbf{L}^{\mathrm{T}}\boldsymbol{x}, \tag{7}$$

$\boldsymbol{f}_{\mathrm{nl}}\left(\boldsymbol{r}, \dot{\boldsymbol{r}}\right)=\left\{f_{\mathrm{nl},1}\left(r_1, \dot{r}_1\right), f_{\mathrm{nl},2}\left(r_2, \dot{r}_2\right), \cdots, f_{\mathrm{nl},\gamma}\left(r_\gamma, \dot{r}_\gamma\right)\right\}^{\mathrm{T}} \in \mathbb{R}^{\gamma\times 1}$ contains the nonlinear force for each nonlinear element and is called the compact nonlinear force vector in this paper. This vector consists only of γ non-zero independent terms corresponding to the number of localised nonlinear elements.

Substituting Eq. (7) into the dynamic equation of Eq. (1), it becomes

$$\mathbf{M}\ddot{\boldsymbol{x}}+\mathbf{C}\dot{\boldsymbol{x}}+\mathbf{K}\boldsymbol{x}+\mathbf{L}\boldsymbol{f}_{\mathrm{nl}}\left(\boldsymbol{r}, \dot{\boldsymbol{r}}\right)=\boldsymbol{p}\left(t\right). \tag{8}$$

Note that the dynamic equation denoted by Eq. (8) is as exact as Eq. (1), since no reduction of the system is performed.

It is common in localised nonlinear structures for the structural responses to be dominated by their primary harmonic terms when sufficient damping exists [8,15,27,30]. Therefore, we only consider updating the nonlinear FE model with measured primary harmonic responses in this paper (as illustrated in Fig. 1). The primary harmonic scalar nonlinear forces can be represented as complex Fourier components, specifically in the form used by [8,15,30]:

$$F_{\mathrm{nl},k}\left(R_k, \mathrm{j}\omega R_k\right)=\frac{\mathrm{j}}{\pi}\int_0^{2\pi} f_{\mathrm{nl},k}\left(r_k, \dot{r}_k\right)e^{-\mathrm{j}\varphi}d\varphi, \quad k=1,2,\dots\gamma, \tag{9}$$

where j is the imaginary unit. R_k and $F_{\mathrm{nl},k}$ denote the primary harmonic term of r_k and $f_{\mathrm{nl},k}$, respectively. ω denotes the frequency of harmonic input, and the generic angle $\varphi=\omega t$.

According to Eq. (7), we have the compact nonlinear force vector expressed in the frequency domain as

$$\boldsymbol{F}_{\mathrm{nl}}\left(\boldsymbol{R},\mathrm{j}\omega\boldsymbol{R}\right)=\left\{F_{\mathrm{nl},1}\left(R_1,\mathrm{j}\omega R_1\right),F_{\mathrm{nl},2}\left(R_2,\mathrm{j}\omega R_2\right),\cdots,F_{\mathrm{nl},\gamma}\left(R_\gamma,\mathrm{j}\omega R_\gamma\right)\right\}^{\mathrm{T}}. \tag{10}$$

Note that while a multi-harmonic representation of $\boldsymbol{F}_{\mathrm{nl}}\left(\boldsymbol{R},\mathrm{j}\omega\boldsymbol{R}\right)$ can be derived [15,30], in this paper we focus on updating the structure with measured primary harmonic components.

Transforming Eq. (8) into frequency domain and extracting the primary harmonic terms, we have

$$\mathbf{D}\boldsymbol{X}+\mathbf{L}\boldsymbol{F}_{\mathrm{nl}}\left(\boldsymbol{R},\mathrm{j}\omega\boldsymbol{R}\right)=\boldsymbol{P},\quad \text{with: } \boldsymbol{R}=\mathbf{L}^{\mathrm{T}}\boldsymbol{X}, \tag{11}$$

where $\boldsymbol{X}$, $\boldsymbol{R}$, $\boldsymbol{P}\in\mathbb{R}^{N\times 1}$ denote the primary harmonic component of responses, relative motion of nonlinear elements and input forces, respectively. The dynamic stiffness matrix is represented by $\mathbf{D}\in\mathbb{R}^{N\times N}$, i.e. $\mathbf{D}=-\omega^2\mathbf{M}+\mathrm{j}\omega\mathbf{C}+\mathbf{K}$ and $\boldsymbol{F}_{\mathrm{nl}}\left(\boldsymbol{R},\mathrm{j}\omega\boldsymbol{R}\right)$ is defined by Eq. (10).

2.2. Equation and output residuals

The purpose of model updating is to minimise discrepancies, typically described in the form of equation or output residuals between analytical predictions and experimental measurements of a structure. The approaches to obtain these residuals play a vital role in the model updating process. For linear structures, we have the well-established force and response residuals [1] and here we extend these to allow the application to nonlinear structures, as illustrated in Fig. 1. This serves as the foundations for the nonlinear model updating strategy presented here. Note that whilst residuals defined on higher order harmonics are mathematically possible, they are beyond the scope of this paper.

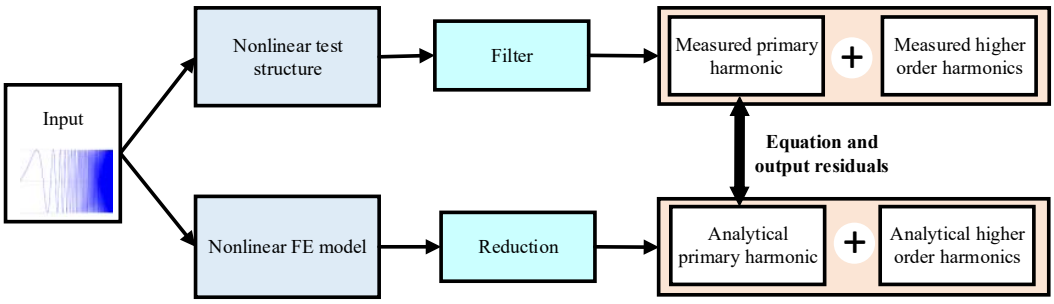

Fig. 1. Illustration of primary harmonic response based equation and output residuals.

2.2.1. Equation residual

The equation residual is defined from the dynamic equation, Eq. (11), as

$$\boldsymbol{\varepsilon}^{\mathrm{ER}} = \boldsymbol{P}^{\mathrm{Exp}} - \mathbf{D}\boldsymbol{X}^{\mathrm{Exp}} - \boldsymbol{F}^{*}, \tag{12}$$

where $\boldsymbol{\varepsilon}^{\mathrm{ER}}$ is the equation residual vector in global physical coordinates. $\boldsymbol{F}^{*}=\mathbf{L}\boldsymbol{F}_{\mathrm{nl}}$ denotes the unknown frequency domain nonlinear force vector to be identified. Vectors $\boldsymbol{P}^{\mathrm{Exp}}$ and $\boldsymbol{X}^{\mathrm{Exp}}$ denote the input forces and responses taken from experimental measurements, and $\mathbf{D}=-\left(\omega^{\mathrm{Exp}}\right)^{2}\mathbf{M}+\mathrm{j}\omega^{\mathrm{Exp}}\mathbf{C}+\mathbf{K}$ denotes the dynamic stiffness matrix of the underlying linear structure calculated at the frequencies used in the test, ω^{Exp}. A physical interpretation of the equation residual is that it represents the input force discrepancy between the test/analysis models.

In practice, we are not able to obtain the full residual vector, $\boldsymbol{\varepsilon}^{\mathrm{ER}}$, as the number of measurement transducers and data acquisition channels are limited. Thus, only spatially incomplete measurements are obtained and consequently the equation residual is partitioned into measured and unmeasured regions, yielding

$$\begin{Bmatrix}\boldsymbol{\varepsilon}_{m}^{\mathrm{ER}}\\ \boldsymbol{\varepsilon}_{u}^{\mathrm{ER}}\end{Bmatrix}=\begin{Bmatrix}\boldsymbol{P}_{m}^{\mathrm{Exp}}\\ \mathbf{0}\end{Bmatrix}-\begin{bmatrix}\mathbf{D}_{mm} & \mathbf{D}_{mu}\\ \mathbf{D}_{um} & \mathbf{D}_{uu}\end{bmatrix}\begin{Bmatrix}\boldsymbol{X}_{m}^{\mathrm{Exp}}\\ \boldsymbol{X}_{u}\end{Bmatrix}-\begin{Bmatrix}\boldsymbol{F}_{m}^{*}\\ \boldsymbol{F}_{u}^{*}\end{Bmatrix}, \tag{13}$$

where the subscripts 'm' and 'u' denote the measured and unmeasured regions, respectively. Note that the input force only exists in the measured region, i.e. $\boldsymbol{P}_{u}=\mathbf{0}\in\mathbb{R}^{N_u\times 1}$, which is quite common during a controlled test.

As indicated by Eq. (13), the measured and unmeasured regions are coupled and the equation residual cannot be obtained only with the measured data. For linear structures, this can be easily overcome by expanding the measured data to the whole region using superposition [1], however this technique is not valid for nonlinear structures. Here, we assume that all the DOFs associated with the nonlinear elements are measured [17,18,20,22,31,32], i.e. $\mathbf{L}_{u}=\mathbf{0}\in\mathbb{R}^{N_u\times 1}$, and the unmeasured part of the FE model do not exhibit errors $\boldsymbol{\varepsilon}_{u}^{\mathrm{ER}}=\mathbf{0}$, such that the measured equation residual $\boldsymbol{\varepsilon}_{m}^{\mathrm{ER}}$ can be reduced to zero provided that the first line of Eq. (13) becomes

$$\boldsymbol{F}_{m}^{*}=\boldsymbol{P}_{m}^{\mathrm{Exp}}-\left(\mathbf{D}_{mm}-\mathbf{D}_{mu}\mathbf{D}_{uu}^{-1}\mathbf{D}_{um}\right)\boldsymbol{X}_{m}^{\mathrm{Exp}}. \tag{14}$$

Note that if $\mathbf{L}_u \neq \mathbf{0} \in \mathbb{R}^{N_u \times 1}$, the equation residual can still be approximated by using reduced FE models and measured responses, see reference [34] for more details.

According to Eq. (14), $\boldsymbol{F}_m^*$ can be calculated at measured channels and the location matrix, $\mathbf{L}_m$, can be determined by observing the locations at which $\boldsymbol{F}_m^*$ is sufficiently large. Next, we allow the candidate nonlinear forces to exist only at the identified nonlinear locations such that the equation residuals, $\boldsymbol{\varepsilon}_m^{\mathrm{ER}}$, will not be reduced to zero but the number of unknown parameters will be significantly reduced for a more robust identification. Noting $\boldsymbol{F}_m^*=\mathbf{L}_m\boldsymbol{F}_{\mathrm{nl}}$, the equation residual can be re-expressed as

$$\boldsymbol{\varepsilon}_m^{\mathrm{ER}} = \boldsymbol{P}_m^{\mathrm{Exp}} - \left(\mathbf{D}_{mm} - \mathbf{D}_{mu}\mathbf{D}_{uu}^{-1}\mathbf{D}_{um}\right)\boldsymbol{X}_m^{\mathrm{Exp}} - \mathbf{L}_m\boldsymbol{F}_{\mathrm{nl}}, \quad \text{with: } \boldsymbol{R}=\mathbf{L}_m^{\mathrm{T}}\boldsymbol{X}_m^{\mathrm{Exp}}, \tag{15}$$

where, at this stage, $\boldsymbol{F}_{\mathrm{nl}}$ is an unknown vector to be identified, $\boldsymbol{R}$ is estimated from measurement and $\mathbf{L}_m$ denotes the location matrix in the measured region.

As indicated by Eq. (15), the equation residual in the measured region, $\boldsymbol{\varepsilon}_m^{\mathrm{ER}}$, can be obtained with an analytical model (which gives partitioned matrices $\mathbf{D}_{mm}$, $\mathbf{D}_{mu}$, $\mathbf{D}_{um}$ and $\mathbf{D}_{uu}$), measured nonlinear responses $\boldsymbol{X}_m^{\mathrm{Exp}}$ and inputs $\boldsymbol{P}_m^{\mathrm{Exp}}$ over a range of excitation frequencies. The major benefit of this approach is that it separates nonlinear forces from a MDOF structure and allows each nonlinear element to be considered independently. This is useful for the localisation, characterisation or initial quantification of the nonlinear elements, although it may be susceptible to bias under non-zero mean noise and modelling errors.

2.2.2. Output residual

An alternative approach is to define a residual based on outputs, aiming to acquire the minimum discrepancy between analytical predicted responses and measured data. Here, two forms of output residuals are defined for nonlinear structures.

(1) Direct form or implicit form

A straightforward form of output discrepancy is to consider the difference between analytical predictions and experimentally measured data [8]

$$\boldsymbol{\varepsilon}^{\mathrm{OR}} = \underbrace{\boldsymbol{X}^{\mathrm{Ana}}\left(\omega^{\mathrm{Exp}}, \boldsymbol{P}^{\mathrm{Exp}}\right)}_{\text{analytical}} - \underbrace{\boldsymbol{X}^{\mathrm{Exp}}\left(\omega^{\mathrm{Exp}}, \boldsymbol{P}^{\mathrm{Exp}}\right)}_{\text{measured}}, \tag{16}$$

where $\boldsymbol{\varepsilon}^{\mathrm{OR}}$ denotes the direct form (or implicit form) of output residual. $\boldsymbol{X}^{\mathrm{Ana}}\left(\omega^{\mathrm{Exp}}, \boldsymbol{P}^{\mathrm{Exp}}\right)$ and $\boldsymbol{X}^{\mathrm{Exp}}\left(\omega^{\mathrm{Exp}}, \boldsymbol{P}^{\mathrm{Exp}}\right)$ denote the analytically predicted responses and the measured data under input $\boldsymbol{P}^{\mathrm{Exp}}$ at frequency points ω^{Exp}.

The major challenge is that the analytical prediction, $\boldsymbol{X}^{\mathrm{Ana}}\left(\omega^{\mathrm{Exp}}, \boldsymbol{P}^{\mathrm{Exp}}\right)$, is an implicit nonlinear function of the input $\boldsymbol{P}^{\mathrm{Exp}}$, which often requires iterative or continuation techniques to calculate. Additionally, multiple solutions may exist for a given frequency, leading to difficulties in automatically correlating these analytical responses with the measurements. Nevertheless, the data in the multiple-solution regions are strongly influenced by the nonlinearities and hence contain valuable information. To address these issues, a semi-analytical form of the output residual is proposed.

(2) Semi-analytical form

Rather than directly computing the analytical responses in Eq. (16), a novel semi-analytical form of output residual is proposed. The idea is to build an output form of the nonlinear dynamic equation with the semi-analytical output residual defined as a residual of this equation.

The output form of the dynamic equation can be obtained by pre-multiplying both sides of Eq. (11) with the linear receptance matrix $\mathbf{H}$,

$$\boldsymbol{X} + \mathbf{H}\mathbf{L}\boldsymbol{F}_{\mathrm{nl}}\left(\boldsymbol{R}, \mathrm{j}\omega\boldsymbol{R}\right) = \mathbf{H}\boldsymbol{P}, \quad \text{where} \quad \mathbf{H} = \left(-\omega^2\mathbf{M} + \mathrm{j}\omega\mathbf{C} + \mathbf{K}\right)^{-1}. \tag{17}$$

Note that the receptance data, as shown in Eq.(17), are often directly measured during tests or superposed by measured underlying linear modes in the frequency range of interest for a large-scale structure [2].

Substituting measured data $\boldsymbol{P}^{\mathrm{Exp}}$, $\boldsymbol{X}^{\mathrm{Exp}}$ and ω^{Exp} into Eq. (17), the semi-analytical output residual, $\boldsymbol{\varepsilon}^{\mathrm{SOR}}$, is defined as

$$\boldsymbol{\varepsilon}^{\mathrm{SOR}} = \underbrace{\boldsymbol{X}^{\mathrm{Semi}}\left(\omega^{\mathrm{Exp}}, \boldsymbol{P}^{\mathrm{Exp}}\right)}_{\text{semi-analytical}} - \underbrace{\boldsymbol{X}^{\mathrm{Exp}}\left(\omega^{\mathrm{Exp}}, \boldsymbol{P}^{\mathrm{Exp}}\right)}_{\text{measured}}, \tag{18}$$

where $\boldsymbol{X}^{\mathrm{Semi}}\left(\omega^{\mathrm{Exp}}, \boldsymbol{P}^{\mathrm{Exp}}\right) = \mathbf{H}\boldsymbol{P}^{\mathrm{Exp}} - \mathbf{H}\mathbf{L}\boldsymbol{F}_{\mathrm{nl}}\left(\boldsymbol{R}, \mathrm{j}\omega^{\mathrm{Exp}}\boldsymbol{R}\right)$ and $\boldsymbol{R} = \mathbf{L}^{\mathrm{T}}\boldsymbol{X}^{\mathrm{Exp}}$. $\boldsymbol{F}_{\mathrm{nl}}\left(\boldsymbol{R}, \mathrm{j}\omega^{\mathrm{Exp}}\boldsymbol{R}\right)$ are determined by the estimated responses, $\boldsymbol{R}$, as well as intrinsic properties such as adjustable nonlinear coefficients that describe the nonlinearities.

Once again, the output residual is partitioned into measured and unmeasured regions giving

$$\begin{Bmatrix} \boldsymbol{\varepsilon}_m^{\mathrm{SOR}} \\ \boldsymbol{\varepsilon}_u^{\mathrm{SOR}} \end{Bmatrix} = \begin{bmatrix} \mathbf{H}_{mm} \\ \mathbf{H}_{um} \end{bmatrix} \boldsymbol{P}_m^{\mathrm{Exp}} - \begin{bmatrix} \mathbf{H}_{mm} & \mathbf{H}_{mu} \\ \mathbf{H}_{um} & \mathbf{H}_{uu} \end{bmatrix} \begin{bmatrix} \mathbf{L}_m \\ \mathbf{L}_u \end{bmatrix} \boldsymbol{F}_{\mathrm{nl}}\left(\boldsymbol{R}, \mathrm{j}\omega^{\mathrm{Exp}}\boldsymbol{R}\right) - \begin{Bmatrix} \boldsymbol{X}_m^{\mathrm{Exp}} \\ \boldsymbol{X}_u \end{Bmatrix}, \tag{19}$$

where $\boldsymbol{\varepsilon}_m^{\mathrm{SOR}}$ and $\boldsymbol{\varepsilon}_u^{\mathrm{SOR}}$ denote the semi-analytical output residuals in the measured and unmeasured region, respectively.

If the nonlinearities do not exist in the unmeasured region, i.e. $\mathbf{L}_u = \mathbf{0}$, the output residual in the measured region, $\boldsymbol{\varepsilon}_m^{\mathrm{SOR}}$, can be expressed using the receptance of the underlying linear FE model and measured responses, as

$$\boldsymbol{\varepsilon}_m^{\mathrm{SOR}} = \underbrace{\boldsymbol{X}_m^{\mathrm{Semi}}\left(\omega^{\mathrm{Exp}}, \boldsymbol{P}^{\mathrm{Exp}}\right)}_{\text{semi-analytical}} - \underbrace{\boldsymbol{X}_m^{\mathrm{Exp}}}_{\text{measured}}, \tag{20}$$

where the semi-analytical predictions $\boldsymbol{X}_m^{\mathrm{Semi}}\left(\omega^{\mathrm{Exp}}, \boldsymbol{P}^{\mathrm{Exp}}\right) = \mathbf{H}_{mm}\boldsymbol{P}_m^{\mathrm{Exp}} - \mathbf{H}_{mm}\mathbf{L}_m\boldsymbol{F}_{\mathrm{nl}}\left(\boldsymbol{R}, \mathrm{j}\omega^{\mathrm{Exp}}\boldsymbol{R}\right)$ with $\boldsymbol{R} = \mathbf{L}_m^{\mathrm{T}}\boldsymbol{X}_m^{\mathrm{Exp}}$.

As shown by Eq. (20), the semi-analytical output residual is defined with every measured response branch even when regions of multiple solutions occur during tests, avoiding the need to manually correlate the analytical predictions with the measured data. The details of this process will be introduced in later examples.

Note that additional reduction is required if $\mathbf{L}_u \neq \mathbf{0}$ [34], although a significant difference from the equation residual is that it is not necessary to assume that the unmeasured output residual, $\boldsymbol{\varepsilon}_u^{\mathrm{SOR}}$, is zero when obtaining Eq. (20) and it is generally believed that if the transducers are well placed, the unmeasured residual should converge to a small value when the measured output residual is reduced to a prescribed value.

An advantage of the output residual approach over the equation residual is that the linear receptance matrix can be directly measured or superposed with measured underlying linear modes. However, the major disadvantage is that the output residual is a highly nonlinear function of the compact nonlinear forces or parameters chosen to update, which may suffer from ill-conditioning and may not converge if too many variables are unknown. As such, the output residual

should be used in the penalty functions to refine the nonlinear coefficients when the locations and types of the nonlinearities are known and the number of adjustable variables is small.

3. Details of the proposed nonlinear model updating strategy

The nonlinear model updating strategy proposed here focuses on the process after detection of nonlinearity, i.e. the frequency response data, in the frequency range of interest, are significantly affected by the nonlinear elements.

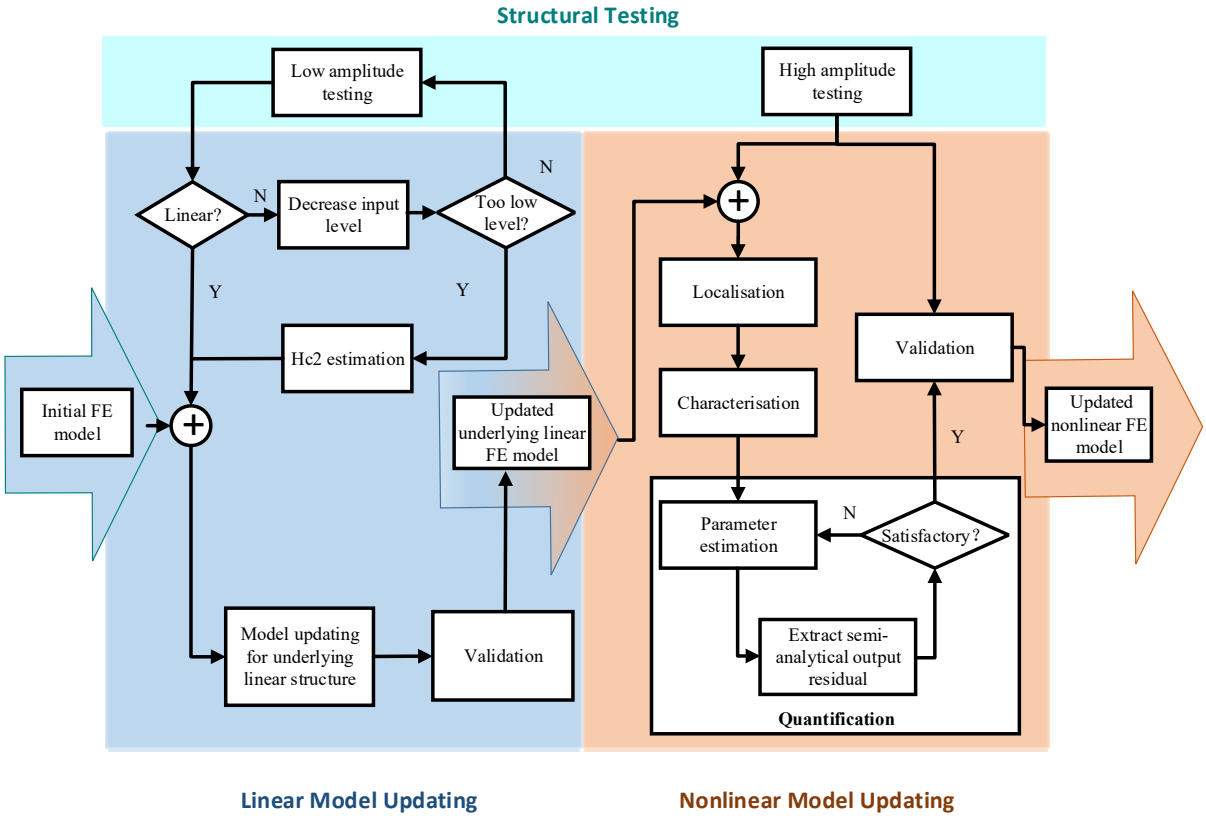

Fig. 2. Flow chart of proposed model updating strategy for local nonlinear structures.

Fig. 2 demonstrates the flow chart for the proposed nonlinear model updating strategy, highlighting the major steps and the data flow between these steps. The strategy consists of three main processes: structural testing, linear model updating and nonlinear model updating. It starts with an initial linear FE model, and followed by a linear model updating process for this underlying linear FE model using low-amplitude test data. With this updated underlying linear

FE model, along with nonlinear responses measured from high-amplitude stepped-sine or swept-sine tests, this strategy continues with a nonlinear model updating process to produce an updated nonlinear FE model. As shown in Fig. 2, an iterative optimisation is used to quantify the nonlinear parameters of the model. The iteration stops once the convergence criteria is satisfied, which is when the changes in objective functions and normalised coefficients fall below a threshold level. This will be discussed in the descriptions of the strategy and illustrated quantitatively in the experimental example. The residuals used during each step of the nonlinear model updating process, as shown in the right side of Fig. 2, are given in Table 1. The various steps included in the updating strategy are now discussed and illustrated with an example.

Table 1

Residuals used for each step during the nonlinear model updating process

	Equation residual	Output residual	
		Semi-analytical form	Direct form
Localisation	√		
Characterisation	√		
Quantification	√ (Initial parameter estimation)	√ (Refined parameter estimation)	
Validation			√

3.1. Experimental data and candidate model

The experimental data required for the updating strategy are measured from two types of test: low-amplitude random or swept-sine excitations that produce homogeneous FRFs; and high-amplitude stepped-sine or slow swept-sine excitation tests that expose the nonlinear responses of the structure. During the low-amplitude tests, the excitation

energy is assumed to be sufficiently low for the underlying linear responses to be obtained. The linear response requirement can be validated by further reducing the input forcing level, observing the homogeneous FRFs and obtaining good coherence functions at these levels. Note that it is challenging to deal with structures that contain clearance or friction nonlinearities since these structures can behave nonlinearly even when the input forcing level is extremely low. For these situations, the conditioned frequency response estimation (H_{c2} estimate) [17] or the pseudo receptance difference method [33] can be used to extract the underlying linear FRFs. The measured frequency range during the low-amplitude tests should cover the modes that are sensitive to the nonlinearities as well as an adequate number of other modes to provide valuable information in updating the underlying linear FE model.

Next, the high-amplitude tests utilise stepped-sine or slow swept-sine excitations to drive the structure into the nonlinear region. Note that: 1) multiple excitation amplitudes are preferred and the highest input level should be able to excite the structure to its maximum in-service energy level; 2) where jumps occur, both forward and backward sweeps are suggested for the same input level; 3) The amplitude of the harmonic forcing does not need to be strictly controlled to a constant value during a sweep, just recorded. It is advantageous to directly measure the nonlinear elements if their locations are pre-known or after localising them.

The data used for the illustrative example were taken from the structure shown in Fig. 3(a) - a 380mm long, 30mm wide clamped beam with a grounded nonlinear mechanism 100mm from the tip. Data were measured at five points a_1 to a_5 with the nonlinear element located at a_2. Fig. 3(b) shows a closer view of the nonlinear mechanism, comprised of two linear springs arranged perpendicular to the nodal movement at the connection point, and Fig. 3(c) shows a schematic of the mechanism. This arrangement produces a geometrically nonlinear element with an additional linear stiffness component [34,35]. Fig. 3(d) shows a linear FE model of the beam using an elastic modulus of 210 GPa, and a nominal thickness of 1mm; the latter will be updated using the low-amplitude test data since adhesive tape was

attached to the surface of the beam to add damping but with the consequence of detuning the effective thickness. The beam was discretised into 15 elements and the measurement was taken at DOFs 3, 9, 13, 19 and 27. Note that the rotational DOFs are not denoted in Fig. 3(d). Lumped masses were added to the DOFs to represent the transducers (12g for each of the five accelerometers and 30g for the force transducer at DOF 27). The shaker was located at a_5 (DOF 27) and its rotational stiffness is to be updated. Flexibility of the boundary is also modelled at DOFs 31 and 32, as shown in Fig. 3(d). The linear stiffness contribution due to the nonlinear mechanism is modelled at a_2 (DOF 9) in the underlying linear FE model but the part of the nonlinear contribution is assumed to be unknown.

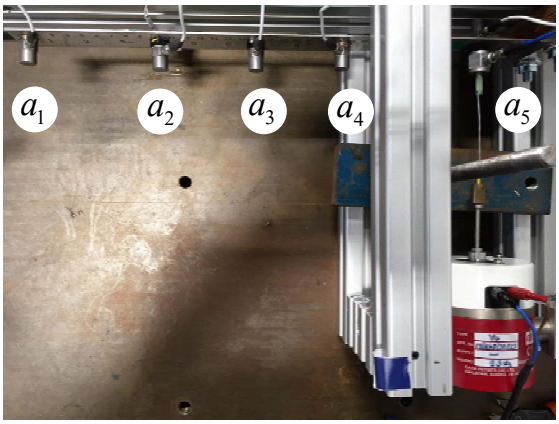

(a)

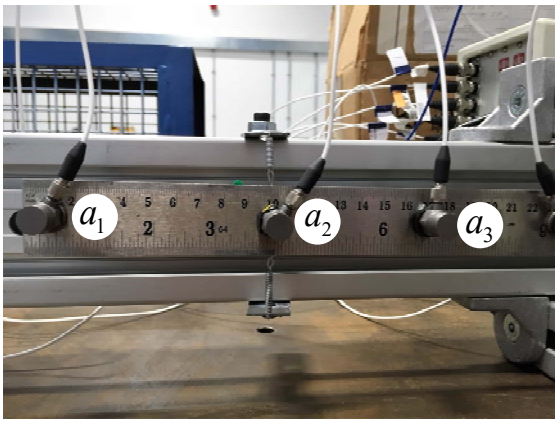

(b)

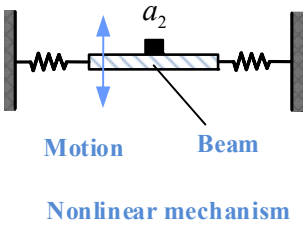

(c)

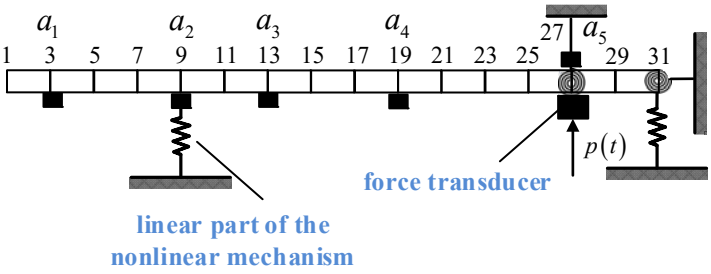

(d)

Fig. 3. The clamped beam experiment: (a) photograph of the test set-up; (b) closer view of the nonlinear mechanism; (c) schematic of the nonlinear mechanism; and (d) linear finite element model constructed in MATLAB.

For this illustrative example, the low-amplitude test data were measured using broadband random excitations at two forcing levels with root mean square (RMS) values of 0.2N and 0.5N. The high-amplitude tests consisted of stepped-sine excitation at three forcing levels (1N, 1.25N and 1.5N) around the first mode of the beam and the primary harmonic responses at five channels were recorded. The results will be demonstrated in Section 3.2 and Section 3.3 in detail when describing the updating steps given in Fig. 2.

3.2. Linear model updating process

Linear model updating is a mature area with a number of commercial software packages available and successful applications to numerous large-scale structures [1,2]. In the proposed strategy, the linear model updating process is based on the measured data under low-amplitude excitation and its detailed process will not be addressed in this paper. Interested readers can refer to references [1] and [2] for more details. We assume that a good model of the underlying linear structure is built with this process such that the modelling errors of the linear FE model are small, i.e. the model exhibits only marginal test/analysis discrepancies in predicting FRFs under low-amplitude excitations.

For the illustrative test structure, the FRFs obtained from the two low-amplitude broadband levels (RMS 0.2N and RMS 0.5N) agree well (peak frequency differences are within the frequency resolution of the measurement), indicating that, at these forcing levels, the structure may be treated as linear. With this confirmed, the 0.5N data is used for the model updating of the underlying linear FE model. The data is shown in Fig. 4(a) as FRFs for the two representative measured locations. Corresponding coherence plots are given in Fig. 4(b), where it can be seen that good coherence is achieved around the resonances with low coherence only near anti-resonances, where the signal-to-noise (S/N) ratio is low.

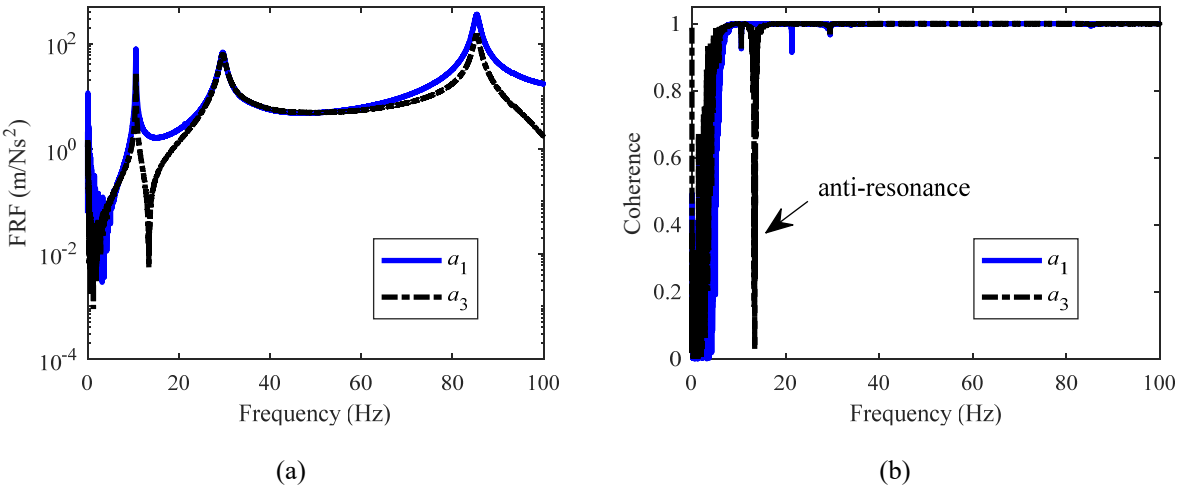

(a) (b)

Fig. 4. Linear FRF data measured at two locations: (a) magnitude and (b) coherence.

The parameters included in the updating and their final values are summarised in Table 2. Note that Rayleigh viscous damping, $\mathbf{C}=\alpha\mathbf{M}+\beta\mathbf{K}$, is assumed for the beam, where α and β are the coefficients of proportional damping.

Table 2

Parameters included in the linear model updating process and the final updated results

Name	Updated value	Name	Updated value
Translational stiffness at the boundary	394.01 kN/m	Linear stiffness component of the nonlinear mechanism	359N/m
Rotational stiffness at the boundary	258.38 N m/rad	Linear damping component of the nonlinear mechanism	1.005×10^{-2} N m s/rad
Rotational stiffness of the stinger	7.48×10^{-2} N m/rad	Proportional damping coefficient, α	2.63e-1
Beam thickness	1.1078 mm	Proportional damping coefficient, β	2.16e-5

Table 3 gives the first three modal frequencies and Fig. 5(a) shows the corresponding mode shape for the measured data and the updated linear FE model. Fig. 5(b) also shows the FRFs around the first mode. These indicate good agreement for all the three modes within the frequency range of interest.

Table 3

Comparison of modal properties between the measurement and the updated linear FE model

	Measured Frequency (Hz)	Updated Frequency (Hz)	Error
First mode	10.5924	10.5895	-0.02702%
Second mode	29.6083	30.3499	2.5048%
Third mode	85.3293	85.7058	0.44125%

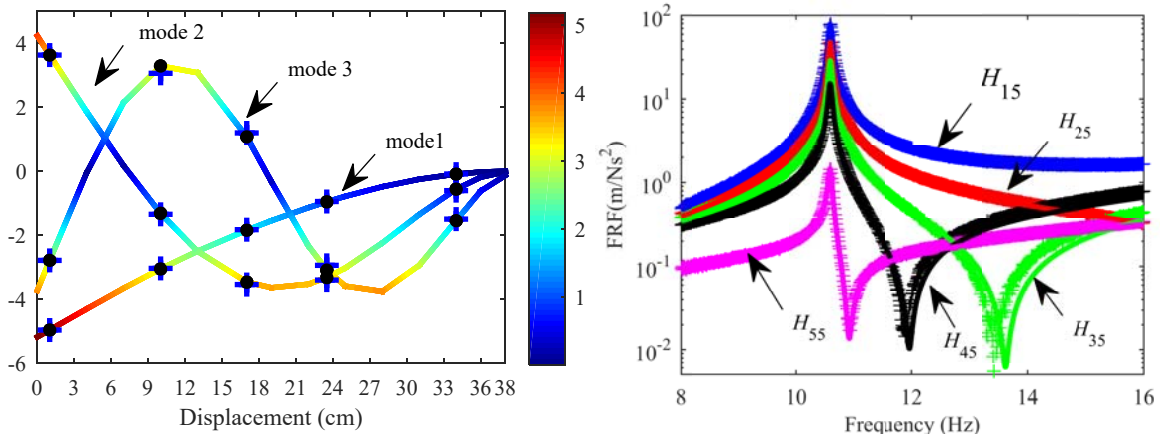

(a) (b)

Fig. 5. Comparison between experimental data (cross points) and numerical results (lines) in terms of (a) mode shapes and (b) linear FRFs around the first mode.

The correlation of the test data and updating linear FE model is good. To confirm this, the Modal Assurance Criterion (MAC) is obtained as

$$\mathrm{MAC}=\begin{bmatrix} 1.0000 & 0.0135 & 0.0203 \\ 0.0107 & 0.9999 & 0.0377 \\ 0.0244 & 0.0519 & 0.9983 \end{bmatrix}, \tag{21}$$

where the diagonal dominance of the matrix indicates good pairing of the analytical and measured modes.

3.3. Nonlinear model updating process

During high-amplitude tests, nonlinear behaviours may lead to distortions of the frequency response data. In this illustrative example, the resonance leans to higher frequencies as the forcing level increases, indicating the hardening nature of the nonlinearity. Jumps are also present during the tests with different jump down and jump up frequencies being observed in the forward and backward sweep data. During the high-amplitude tests, the first mode appeared to be nonlinear and was most sensitive to any physical adjustments of the nonlinear mechanism. The nonlinear updating process uses the nonlinear frequency response data under stepped-sine inputs around this resonance (from 10Hz-13Hz). Fig. 6 shows typical acceleration response functions recorded at location a_4 (DOF 19 in Fig. 3(d)) for forward and backward stepped-sine excitations. It shows that the updated underlying linear FE model only agrees very well with the low-amplitude test results. In contrast, responses from large-amplitude excitation deviate from the linear predictions demonstrating that the linear model is not sufficient to describe the amplitude-dependent characteristics nor the jump phenomena observed at high-amplitude excitations.

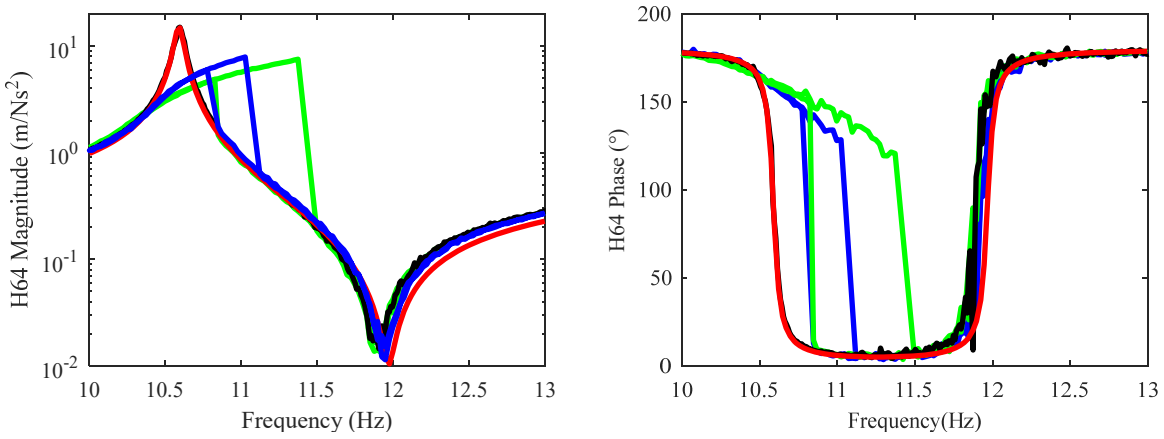

(a) (b)

Fig. 6. Comparison of linear and nonlinear acceleration response functions at location a_4. (a) Magnitude and (b) phase: (——) measured from 1N excitation, (——) measured from 1.5N excitation, (——) measured from low-amplitude excitation, and (——) analytical linear FE model.

The linear model is now extended to capture the nonlinear behaviours by using the high-amplitude excitation data to model and update the nonlinear part of the connection mechanism. In the example considered here, data from four sweeps (forward and backward sweeps of 1N and 1.5N) are used in the quantification step, and data from further two sweeps (both forward and backward sweeps of 1.25N) will be reserved for use purely in the validation step. The nonlinear updating process is shown on the right-hand side of Fig. 2 and the basic equations behind the process will be introduced as follows.

3.3.1. Localisation

The aim of the localisation step is to obtain the location matrix $\mathbf{L}$ that distributes the compact nonlinear force vector $\boldsymbol{f}_{\mathrm{nl}}\left(\boldsymbol{r},\dot{\boldsymbol{r}}\right)$ into the whole structural region as $\boldsymbol{f}^{*}\left(\boldsymbol{x},\dot{\boldsymbol{x}}\right)$, see Eq. (7). The localisation of the nonlinear elements is not only key to adding nonlinear behaviours to the underlying linear dynamics, but also provides information regarding where to add additional nonlinear elements to further upgrade the linear FE model.

For certain systems, the locations of the nonlinear elements are known, such as assembled nonlinear mechanisms [5,17] and joints[8-10], so this step is straightforward; however, the locations are generally unknown. In this case, it is proposed that the measured nonlinear force vector $\boldsymbol{F}_{m}^{*}$ is obtained by Eq. (14). An index vector of nonlinear forces in the measured region is defined as the sum of magnitudes of nonlinear forces over the measured frequencies, written as

$$\boldsymbol{I}_{\boldsymbol{F}_{m}^{*}}=\sum_{i=1}^{N_f}\left|\boldsymbol{F}_{m}^{*}\left(\omega_{i}^{\mathrm{Exp}}\right)\right|, \tag{22}$$

where $\omega_{i}^{\mathrm{Exp}}\left(i=1,2,\ldots N_{f}\right)$ denotes the selected measured frequencies around nonlinear resonances, where the structural behaviours are highly affected by nonlinear elements [34], N_f is the number of selected frequency points. The locations of nonlinearities will correspond to those measured DOFs with sufficiently high indices. If the nonlinear forces exist in the unmeasured region, a reduction of the linear FE model is required and the index of nonlinear forces,

as defined by Eq. (22), can also be obtained with a reduced model [34]. Note that, where a significant nonlinearity exists, transducers should be placed to ensure the measured data sufficiently capture the nonlinearity.

For the illustrative test structure, the location of this nonlinear element is obtained by extracting nonlinear forces at five measured DOFs using Eq. (14) and calculated for each channel using Eq. (22). Note that the measured data is filtered with a threshold of 5m/s^2 minimum acceleration deviation between the linear responses and measured nonlinear data in at least one channel. This threshold is utilised to filter the data for the localisation step as well as characterisation and quantification steps to improve the robustness of the entire updating process. Interested readers can refer to reference [34] for more details. The location matrix is identified as a single grounded nonlinearity at DOF 9, i.e.

$$\mathbf{L} = \begin{bmatrix} 0 & \dots & \underset{9\text{th}}{1} & 0 & \dots & 0 \end{bmatrix}^{\mathrm{T}}. \tag{23}$$

As shown in Fig. 3(d), this is the true location of the nonlinear element

3.3.2. Characterisation

The purpose of the characterisation step is to determine the types of nonlinearities present, in terms of suitable and adequate mathematical descriptions. If the type of nonlinearity is already known, for examples see references [36] and [37], this step is not necessary. For real-life structures, however, the form of nonlinearities present is unlikely to be known in advance, thus they should be determined or confirmed using measured data. In the strategy presented here, we extend the single-degree-of-freedom (SDOF) Equivalent Dynamic Stiffness mapping technique [38] for nonparametric characterisation of MDOF systems.

With the known or identified location matrix, $\mathbf{L}$, we can significantly reduce the complexity of the characterisation step by investigating just a few non-zero terms, $\boldsymbol{F}_{\mathrm{nl}}\left(\boldsymbol{R}, \mathrm{j}\omega\boldsymbol{R}\right) \in \mathbb{R}^{\gamma\times 1}$, instead of the full measured nonlinear force vector $\boldsymbol{F}_m^*$.

The compact nonlinear force vector is extracted by minimising the equation residual, $\boldsymbol{\varepsilon}_m^{\mathrm{ER}}$, defined by Eq. (15). This is achieved by using

$$\hat{\boldsymbol{F}}_{\mathrm{nl}}(\omega_i)=\arg\min_{\boldsymbol{F}_{\mathrm{nl}}}\left|\boldsymbol{\varepsilon}_m^{\mathrm{ER}}(\omega_i)\right|^2,\quad i=1,2,\ldots N_f, \tag{24}$$

where $\hat{\boldsymbol{F}}_{\mathrm{nl}}(\omega_i)$ denotes estimated value of $\boldsymbol{F}_{\mathrm{nl}}$ at frequency point ω_i. N_f is the number of measured frequency points.

Eq. (24) can be solved iteratively using a sensitivity analysis [8] or with optimisation. As $\hat{\boldsymbol{F}}_{\mathrm{nl}} \in \mathbb{R}^{\gamma\times 1}$ is estimated using data from N_m channels, Eq. (24) is normally an over-determined equation, since the number of transducers is assumed to be larger than that of independent nonlinear elements, i.e. $\gamma \le N_m$. If this inequality is not satisfied, i.e. if very few transducers are used, Eq. (24) would become ill-conditioned and a regularisation process should be employed [1,8].

For the illustrative test structure, the nonlinear force at a_2 is obtained according to Eq. (24) by using the measured data at the same location, as shown in Fig. 7 .

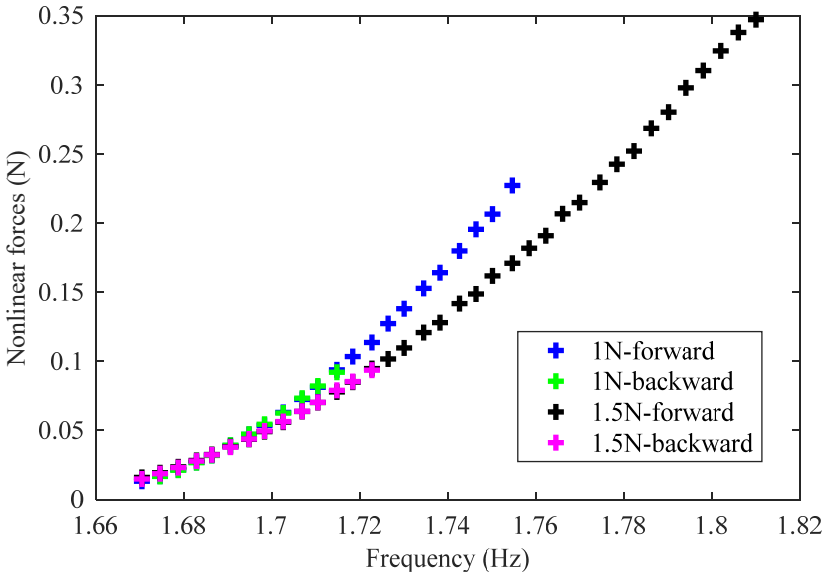

Fig. 7. Nonlinear forces extracted at location a_2, DOF9.

Now that the compact nonlinear force vector $\hat{\boldsymbol{F}}_{\mathrm{nl}}$ has been obtained and its corresponding relative motions, $\boldsymbol{R}$, can be calculated using Eq. (15). Following this, the Equivalent Dynamic Stiffness mapping technique [38] is applied

for each nonlinear element. The equivalent dynamics stiffness is defined as the complex ratio between the nonlinear force and the displacement response of a nonlinear element. For the *k*th nonlinear element, this can be written as

$$D_{\text{stiff},k}\left(\omega^{\text{Exp}},\bar{R}_k\right)=\frac{\hat{F}_{\text{nl},k}}{R_k},\quad k=1,2,\ldots\gamma, \tag{25}$$

where $\hat{F}_{\text{nl},k}$ and R_k denote the *k*th term in the compact nonlinear force vector, $\hat{\boldsymbol{F}}_{\text{nl}}$, and its corresponding relative motion vector, $\boldsymbol{R}$, respectively. $\bar{R}_k$ denotes the magnitude of R_k and ω^{Exp} denotes the measured frequency points $\omega_1,\omega_2,\ldots\omega_{N_f}$.

The real and imaginary parts of the equivalent dynamic stiffness, $D_{\text{stiff},k}$, correspond to the stiffness and damping of the *k*th nonlinear element, respectively. They can be plotted as discrete points in a three-dimensional space over displacement amplitude $\bar{R}_k$ and frequency ω. These points will form a repeatable surface as the equivalent dynamic stiffness is a function only of $\bar{R}_k$ and ω, as demonstrated in reference [38]. A nonparametric surface-fitting of these points with selected basis functions is then performed to reveal the types of nonlinear elements present.

The equivalent dynamic stiffness for the nonlinear element in the example is obtained by using Eq. (25) and its real part is shown in Fig. 8 as scatter points. It can be seen that this force increases with the response amplitude, thereby two kinds of polynomial groups with amplitude-dependent terms are considered here: a three-term fit (basis function chosen as $\{1,\bar{R},\bar{R}^2\}$) and a two-term fit (basis function chosen as $\{1,\bar{R}^2\}$). The results are shown in Fig. 8 and a visual inspection suggests that the two-term fit is already sufficient to characterise the nonlinear element. Therefore, the nonlinear part of the connection mechanism is characterised as a cubic nonlinear spring with a small linear component (cubic spring $f\propto r^3$ introduces $\text{Re}\left(D_{\text{stiff}}\right)\propto\bar{R}^2$ [34])

$$\text{Re}\left(D_{\text{stiff}}\right)=\theta_1+\theta_2\bar{R}^2, \tag{26}$$

where θ_1 and θ_2 are unknown coefficients to be estimated. Note that the linear component would ideally be zero, with the linear dynamics completely captured in the linear updating process. Here, this term is non-zero, but small to represent a correlation to the linear part of the nonlinear mechanism that has already been modelled in the linear FE model.

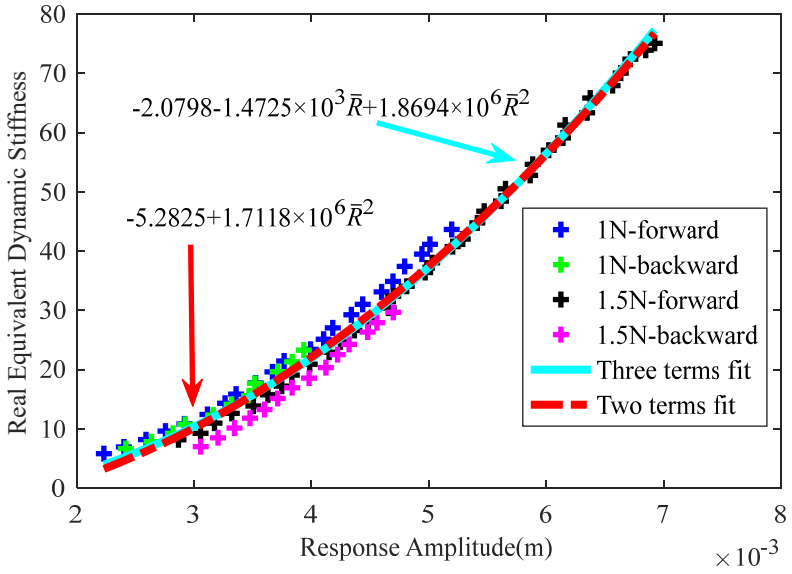

Fig. 8. Real Equivalent Dynamic Stiffness plot: Projection to the $\mathrm{Re}\left(D_{\mathrm{stiff}}\right)-\bar{R}$ plane.

The imaginary part of the equivalent dynamic stiffness, which corresponds to the damping of the nonlinear mechanism, is small and no clear trend can be observed. We note that the real part of D_{stiff} is at least an order larger than the imaginary part, as shown in Fig. 9. Therefore, a small error in the measured phases may result in a bias on the damping estimation at this stage.

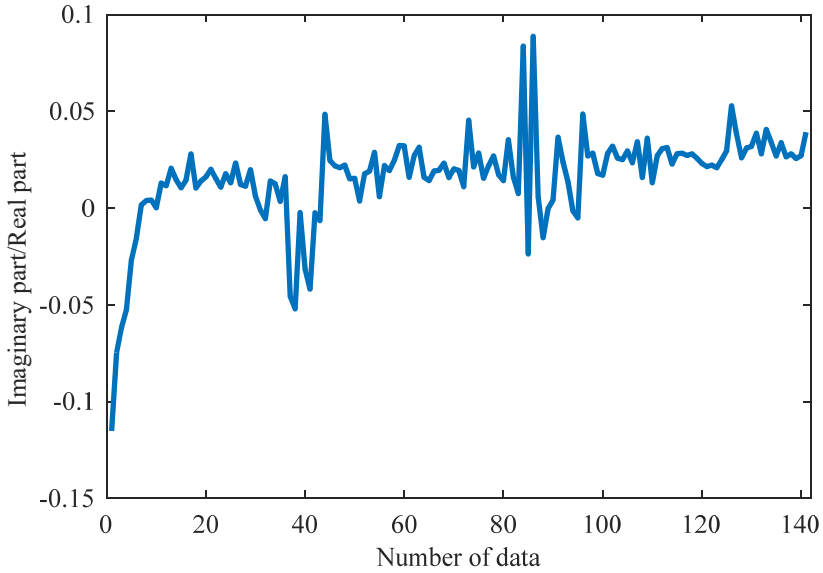

Fig. 9. Ratio of magnitudes between the imaginary and the real part of the obtained equivalent dynamic stiffness.

A detailed and rigorous characterisation of the nonlinear damping for a mechanism with very light damping such as the one present in this illustrative structure is beyond the scope of this paper. Here, we use a typical quadratic damping model to fit the data (quadratic damping $f \propto |\dot{r}|\dot{r}$ introduces $\mathrm{Im}\left(D_{\mathrm{stiff}}\right) \propto \omega^2 \bar{R}$), i.e.,

$$\mathrm{Im}\left(D_{\mathrm{stiff}}\right) = \theta_3 \omega^2 \bar{R}, \tag{27}$$

where θ_3 is the unknown damping coefficient. The fitting results are shown in Fig. 10 and reveal that the damping data from the measurement are complicated, thus refinement of the damping model is needed during the quantification step.

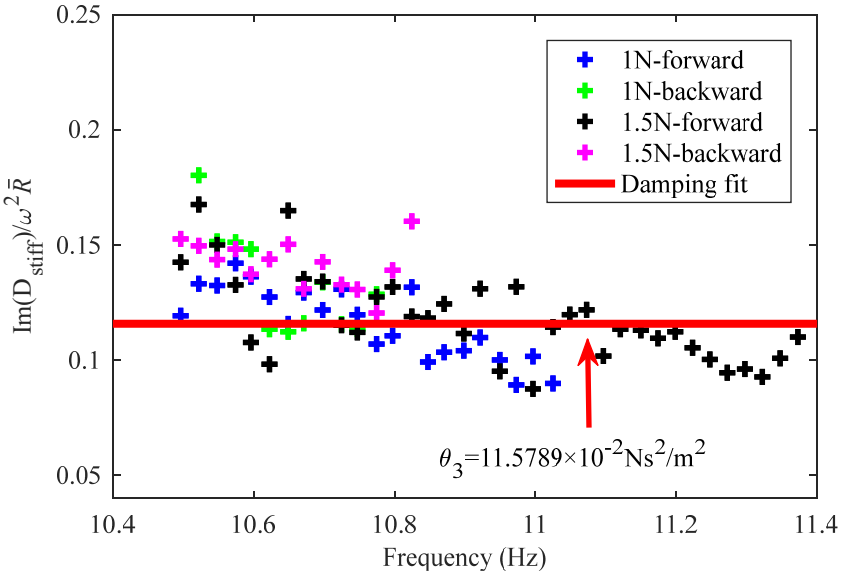

Fig. 10. Parametric fit of the damping model of Eq. (27).

3.3.3. Quantification

The quantification step in this strategy is the process of refining the initial parameter estimates, found in the characterisation step using equation residuals, by minimising the semi-analytical output residuals.

In general, the characterisation step has resulted in the functions

$$\mathrm{Re}\left(D_{\mathrm{stiff},k}\right) = \mathrm{g}_k^{\mathrm{real}}\left(\omega, \bar{R}_k, \theta_{1,k}^{\mathrm{real}}, \theta_{2,k}^{\mathrm{real}}, \cdots, \theta_{\tau_k,k}^{\mathrm{real}}\right), \quad k = 1,2,\ldots\gamma, \tag{28}$$

$$\mathrm{Im}\left(D_{\mathrm{stiff},k}\right) = \mathrm{g}_k^{\mathrm{imag}}\left(\omega, \bar{R}_k, \theta_{1,k}^{\mathrm{imag}}, \theta_{2,k}^{\mathrm{imag}}, \cdots, \theta_{\upsilon_k,k}^{\mathrm{imag}}\right), \quad k = 1,2,\ldots\gamma, \tag{29}$$

where $D_{\text{stiff},k}$ was calculated using Eq. (25) from the measured data. $\mathrm{g}_k^{\text{real}}$ and $\mathrm{g}_k^{\text{imag}}$ denote the basis functions used to fit the real and imaginary parts of $D_{\text{stiff},k}$, respectively.

Therefore, the equivalent dynamic stiffness of *k*th nonlinear element can be denoted by

$$g_k = g_k^{\text{real}} + \mathrm{j} g_k^{\text{imag}}. \tag{30}$$

The basis functions are identified in the characterisation step with an initial estimates of $\theta_{1,k}^{\text{real}}$ to $\theta_{\tau_k,k}^{\text{real}}$ and $\theta_{1,k}^{\text{imag}}$ to $\theta_{\upsilon_k,k}^{\text{imag}}$ fitted through a least-squares process based on the measured real and imaginary parts of the equivalent dynamic stiffness points (see Fig. 8 and Fig. 10). τ_k and υ_k denote the number of coefficients required to describe the stiffness and damping model of *k*th nonlinear element, respectively. Note that actual measurements are polluted with noise and thereby the initial estimates of the nonlinear coefficients obtained in the characterisation step may be biased.

For the illustrative test structure, Eq. (30) may be written as

$$g = \theta_1 + \theta_2 \overline{R}^2 + \mathrm{j}\theta_3 \omega^2 \overline{R}, \tag{31}$$

with the initial estimation of the coefficients, shown in Fig. 8 and Fig. 10, as

$$\theta_1 = -5.2825\,\mathrm{N/m}, \quad \theta_2 = 1.7718\times 10^6\,\mathrm{N/m^3}, \quad \theta_3 = 11.5789\times 10^{-2}\,\mathrm{Ns^2/m^2}. \tag{32}$$

The model quality is now improved by minimising the semi-analytical output residual through adjustment to the initially quantified nonlinear coefficients such that the discrepancies between analytically predicted responses and measured data are minimised. After initial parameter estimation, we can group the equivalent dynamic stiffness of all the nonlinear elements, using Eqs. (28) to (30), in an equivalent dynamic stiffness matrix

$$\boldsymbol{D}_{\text{nl}} = \text{diag}\left\{g_1, g_2, \cdots, g_\gamma\right\}, \tag{33}$$

which, following Eqs. (6), (10) and (25), yields

$$\boldsymbol{F}_{\text{nl}} = \boldsymbol{D}_{\text{nl}} \boldsymbol{R}. \tag{34}$$

As the types of the nonlinearities are known at this stage, the semi-analytical output residual denoted by Eq. (20) can be written as

$$\boldsymbol{\varepsilon}_m^{\mathrm{SOR}} = \mathbf{H}_{mm}\boldsymbol{P}_m^{\mathrm{Exp}} - \mathbf{H}_{mm}\mathbf{L}_m\boldsymbol{D}_{\mathrm{nl}}\left(\boldsymbol{\theta},\bar{\boldsymbol{R}}\right)\boldsymbol{R} - \boldsymbol{X}_m^{\mathrm{Exp}}, \text{ with: } \boldsymbol{R}=\mathbf{L}_m^{\mathrm{T}}\boldsymbol{X}_m^{\mathrm{Exp}}, \tag{35}$$

where $\bar{\boldsymbol{R}}$ is the amplitude of relative motion vector, i.e. $\bar{\boldsymbol{R}}=\left\{\bar{R}_1,\bar{R}_2,\ldots\bar{R}_\gamma\right\}^{\mathrm{T}}$, $\boldsymbol{\theta}$ is the nonlinear coefficient vector

$$\boldsymbol{\theta}^{\mathrm{T}} = \{\underbrace{\theta_{1,1}^{\mathrm{real}},\theta_{2,1}^{\mathrm{real}},\cdots,\theta_{\tau_1,1}^{\mathrm{real}},\theta_{1,1}^{\mathrm{imag}},\theta_{2,1}^{\mathrm{imag}},\cdots,\theta_{\upsilon_1,1}^{\mathrm{imag}}}_{\textit{first nonlinear element}},\ldots,\underbrace{\theta_{1,\gamma}^{\mathrm{real}},\theta_{2,\gamma}^{\mathrm{real}},\cdots,\theta_{\tau_\gamma,\gamma}^{\mathrm{real}},\theta_{1,\gamma}^{\mathrm{imag}},\theta_{2,\gamma}^{\mathrm{imag}},\cdots,\theta_{\upsilon_\gamma,\gamma}^{\mathrm{imag}}}_{\textit{last nonlinear element}}\}, \tag{36}$$

and contains adjustable variables to be refined.

Now the coefficient vector $\boldsymbol{\theta}$ will be adjusted to minimise the objective function

$$J_{\boldsymbol{\theta}} = \sum_{i=1}^{N_f}\left|\boldsymbol{\varepsilon}_m^{\mathrm{SOR}}\left(\omega_i\right)\right|^{\mathrm{T}}\mathbf{W}_{\varepsilon^{\mathrm{out}}}\left(\omega_i\right)\left|\boldsymbol{\varepsilon}_m^{\mathrm{SOR}}\left(\omega_i\right)\right|, \tag{37}$$

where $\mathbf{W}_{\varepsilon^{\mathrm{out}}}$ is a real-valued weighting matrix [2] and the coefficients are normalised as

$$\boldsymbol{\theta} = \mathbf{W}_{\boldsymbol{\theta}}\tilde{\boldsymbol{\theta}}, \tag{38}$$

where $\mathbf{W}_{\theta}$ is a normalisation matrix [1], which is used to ensure that the terms in the vector $\tilde{\boldsymbol{\theta}}$ are of the same order.

Mathematically, the nonlinear model may be refined by finding the solution for

$$\hat{\boldsymbol{\theta}} = \arg\min_{\tilde{\boldsymbol{\theta}}} J_{\boldsymbol{\theta}}\left(\tilde{\boldsymbol{\theta}}\right), \tag{39}$$

where $\hat{\boldsymbol{\theta}}$ denotes the refined estimates of the nonlinear coefficients. Note that the penalty function $J_{\boldsymbol{\theta}}$ is highly nonlinear with respect to the normalised coefficient vector $\tilde{\boldsymbol{\theta}}$. Therefore, the number of adjustable nonlinear coefficients, $\mathrm{size}\left(\boldsymbol{\theta}\right)$, should be kept as small as possible. Indeed, $J_{\boldsymbol{\theta}}$ contains N_m channels of frequency responses at N_f measured frequency points, thus,

$$\mathrm{size}\left(\boldsymbol{\theta}\right) << N_m \times N_f, \tag{40}$$

should be satisfied to form an over-determined estimation. Eq. (37) can be minimised through an iterative process until the nonlinear coefficients converge and the objective function is reduced to a prescribed value.

Consider the illustrative example, the nonlinear coefficient vector of the test structure comprises of three terms according to Eq. (31), $\boldsymbol{\theta}=\left[\theta_1,\theta_2,\theta_3\right]^{\mathrm{T}}$, with its initial value denoted by Eq. (32). The semi-analytical output residual, defined by Eq. (35), can be expressed for this beam as

$$\begin{Bmatrix}\varepsilon_3^{\mathrm{SOR}}\\ \varepsilon_9^{\mathrm{SOR}}\\ \varepsilon_{13}^{\mathrm{SOR}}\\ \varepsilon_{19}^{\mathrm{SOR}}\\ \varepsilon_{27}^{\mathrm{SOR}}\end{Bmatrix}=\begin{bmatrix}H_{3,27}\\ H_{9,27}\\ H_{13,27}\\ H_{19,27}\\ H_{27,27}\end{bmatrix}P^{Exp}-\begin{bmatrix}H_{3,9}\\ H_{9,9}\\ H_{13,9}\\ H_{19,9}\\ H_{27,9}\end{bmatrix}\left(\theta_1+\theta_2\bar{R}_9^2+\mathrm{j}\theta_3\left(\omega^{Exp}\right)^2\bar{R}_9\right)R_9-\begin{Bmatrix}X_3^{\mathrm{Exp}}\\ X_9^{\mathrm{Exp}}\\ X_{13}^{\mathrm{Exp}}\\ X_{19}^{\mathrm{Exp}}\\ X_{27}^{\mathrm{Exp}}\end{Bmatrix},\ \text{with: } R_9=X_9^{\mathrm{Exp}}, \tag{41}$$

where P^{Exp} is the input force and $\bar{R}_9$ denotes the amplitude of R_9.

To define the penalty function for the semi-analytical output residual, Eq. (37), the normalisation matrix, $\mathbf{W}_\theta$, and the weighting matrices, $\mathbf{W}_{\varepsilon^{\mathrm{out}}}$, are chosen as

$$\mathbf{W}_\theta=\mathrm{diag}\left[1,\quad 1\times10^{6},\quad 1\times10^{-2}\right], \tag{42}$$

$$\mathbf{W}_{\varepsilon^{\mathrm{out}}}=\begin{cases}\mathrm{diag}\left[100,\quad 100,\quad 100,\quad 100,\quad 100\right], & 11\mathrm{Hz}\le f\le 11.5\mathrm{Hz},\\ \mathrm{diag}\left[1,\quad 1,\quad 1,\quad 1,\quad 1\right], & \text{other.}\end{cases} \tag{43}$$

The normalisation matrix $\mathbf{W}_\theta$, defined by Eq. (42), ensures the terms in vector $\tilde{\boldsymbol{\theta}}$ are of the same order according to the initial values given in Eq. (32). The weighting matrices, $\mathbf{W}_{\varepsilon^{\mathrm{out}}}$ expressed by Eq. (43), are selected to place emphasis on the data near the nonlinear resonance, and they will be further explained in Section 4.1.

The MATLAB optimisation toolbox is employed to minimise Eq. (37) with the tolerance of objective function change set to 1×10^{-4} and the tolerance of minimum normalised coefficient change set to 1×10^{-2}. The optimisation was carried out on an Intel Core i7-4510U machine with Windows10-64 bit operating system and performed a total of 87 iterations of the coefficient vectors in just 12.04 seconds. The evolution of the objective function and one of the normalised coefficients are shown in Fig. 11(a) and (b).

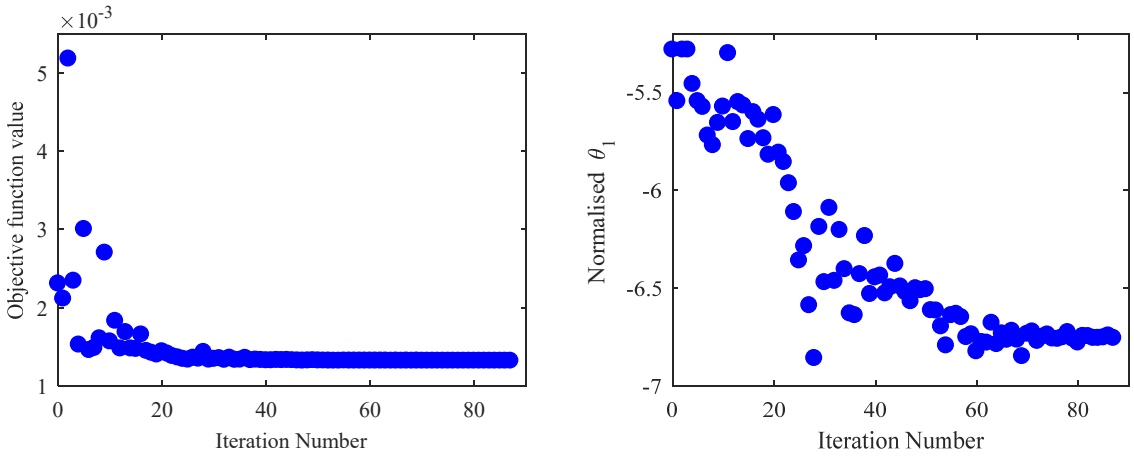

(a) (b)

Fig. 11. Evolution of parameters during the iterations. (a) Objective function values; and (b) $\tilde{\theta}_1$ -normalised θ_1 -values.

After the optimisation, the refined values of the nonlinear coefficients are

$$\boldsymbol{\theta} = \left[-6.7571\,\mathrm{N/m}, \quad 1.7395\times10^{6}\,\mathrm{N/m^3}, \quad 8.7415\times10^{-2}\,\mathrm{Ns^2/m^2} \right]^{\mathrm{T}}. \tag{44}$$

Compared to the results of initial parameter estimation, the value of the objective function drops 42.88% and the nonlinear coefficients θ_1 , θ_2 and θ_3 change by 27.9%, 1.8% and 24.5%, respectively.

We also performed a robustness analysis of this optimisation process by increasing and decreasing the initial parameters by 50% and 25%. It was observed that all these initial parameters converge to within 0.1% difference of the corresponding values given in Eq. (44). The scenario of updating the model using just one set of the high level data (1.5N input) was also investigated and only a maximum of 3.6% difference in coefficient compared to the values given in Eq. (44) was observed.

3.3.4. Validation

The validation step for the nonlinear FE model is first carried out by comparing the direct form of output residual defined by Eq. (16), as summarised in Table 1. In this step, the analytically predicted responses are obtained by solving

the nonlinear dynamic equation of the updated model. Secondly, the capability of the updated model in predicting responses that are not contained in the updating, is assessed.

Fig. 12(a)-(d) compare the responses from the measurement and the updated nonlinear FE model at 1N and 1.5N input levels. It is clearly shown that with the updated nonlinear element, the nonlinear FE model agrees very well with the measured data under high-amplitude excitations (1N and 1.5N).

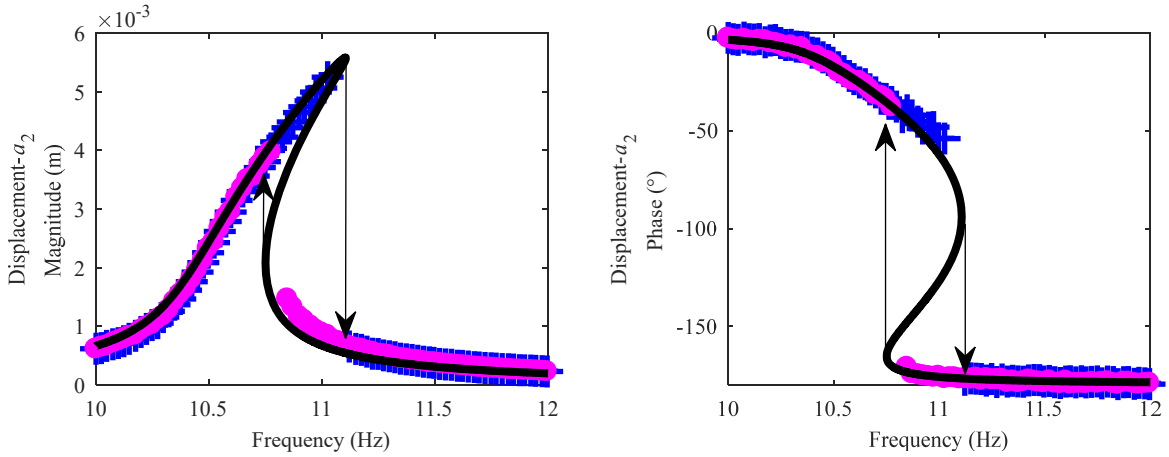

(a) (b)

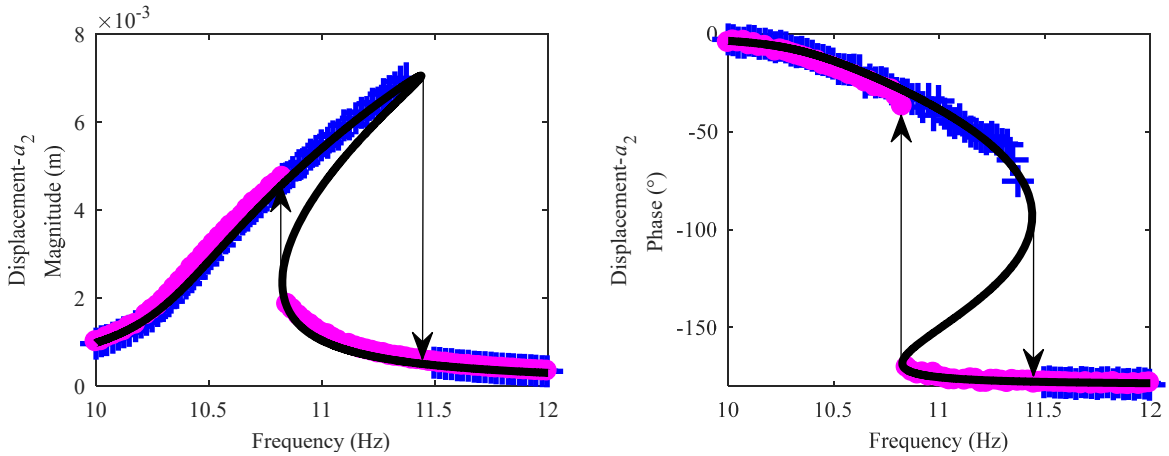

(c) (d)

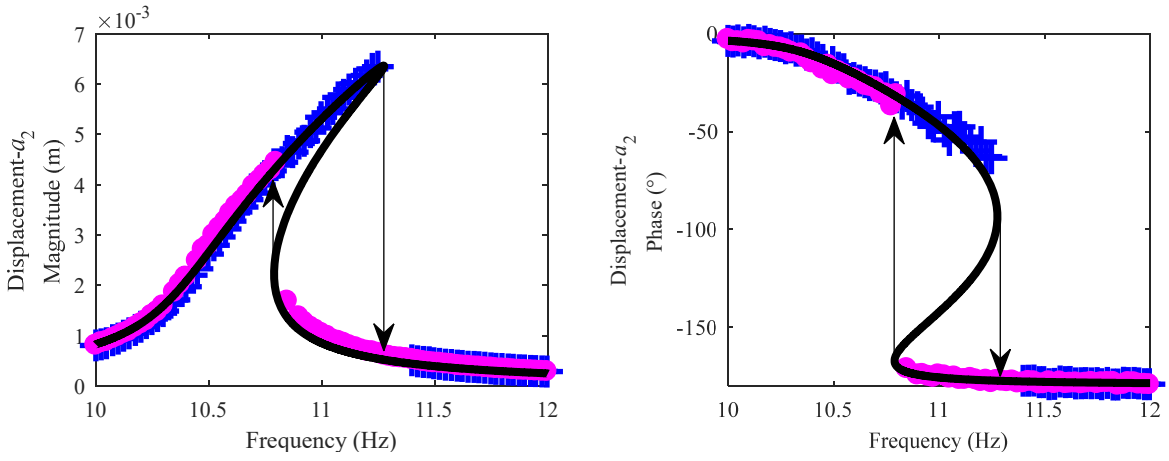

(e) (f)

Fig. 12. Comparison between measured data and analytical predictions of the updated nonlinear FE model at location a_2. The plots show (a) magnitude for 1N input; (b) phase for 1N input; (c) magnitude for 1.5N input; (d) phase for 1.5N input; (e) magnitude for 1.25N input and (f) phase for 1.25N input, where (+) and (●) denote the measured data for the forward and backward sweeps, respectively, and black line denotes analytical responses.

The validation step continues by comparing responses between the measurement and the updated nonlinear FE model using data that has not been used to update the model. Fig. 12(e) and (f) show the 1.25N response data and model predictions demonstrating good agreement.

4. Discussions

4.1 Damping estimation

The damping force is typically much smaller than its stiffness counterpart but plays a significant role in structural dynamic responses. This is demonstrated in Fig. 13 where the damping coefficient θ_3 is reduced in magnitude to 50% and 30% and also increased by 50% of its final updated value.

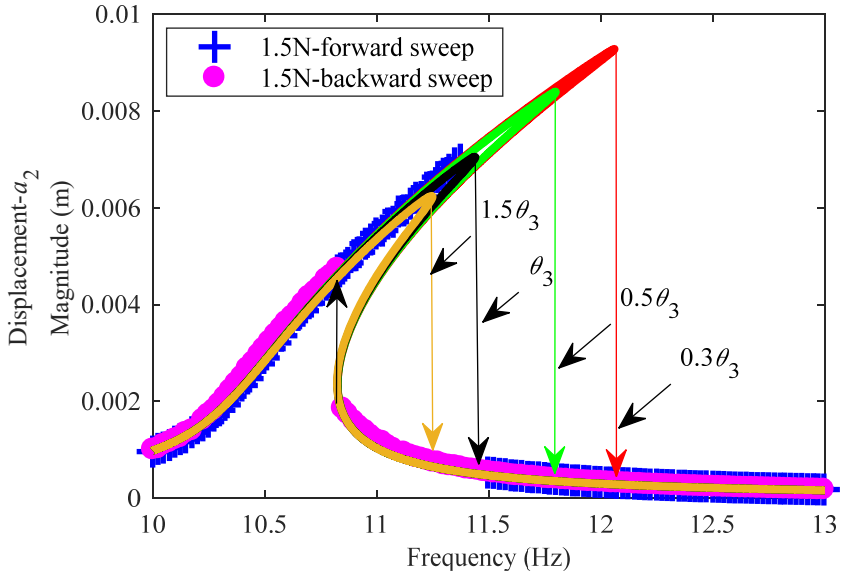

(a)

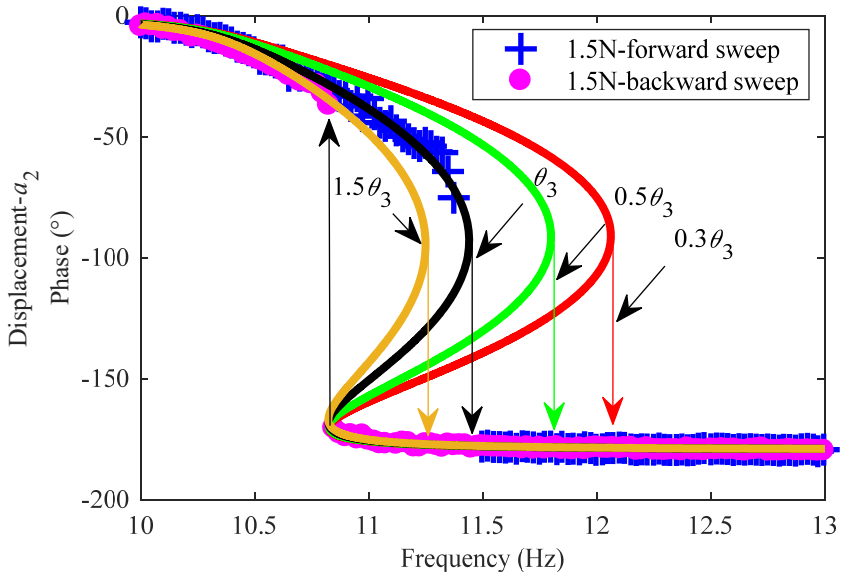

(b)

Fig. 13. Comparison of responses of different estimation of damping levels. The two plots show (a) magnitude and (b) phase, where lines denote analytical responses.

It can be seen in Fig. 13(a) that the magnitudes of analytical responses, in the measured frequency range, are not sensitive to the damping level if the damping is underestimated in the analytical model, since the two models with low

damping can agree very well with the magnitudes of the measured data. If damping in the analytical model is higher than the true level, it may fail to capture the higher amplitudes of the measured responses. This indicates that methods only using residuals of response magnitudes are not likely to have an accurate estimation of the damping. In contrast, as shown in Fig. 13(b), the phases of analytical response are sensitive to the damping level, especially those points close to quadrature (close to -90°). As such, giving additional weighting to the measured responses close to nonlinear resonances can improve the accuracy of damping estimation of the model. This observation justifies the weighting applied via $\mathbf{W}_{\varepsilon^{out}}$ in the semi-analytical output residual in the range from 11Hz to 11.5Hz for the illustrative test structure, as denoted by Eq. (43). It also demonstrates that for a successful damping estimation of nonlinear structures, the objective function should contain the phase.

4.2 Amplitude-varying force input

Without the use of a tightly and slowly controlled forcing input, it is often observed in real testing practice that the amplitude of force excitation varies with frequency. This is not a significant problem for linear structures owning to the homogeneity of linear FRFs; however, it is quite challenging for a nonlinear structure where the response is not linearly proportional to the forcing. For example, if a shaker is supplied with a constant-amplitude sinusoidal voltage, it is typically observed that the forcing amplitude decreases near the resonance [39]. This is due to the coupling of the structure and shaker and is often referred as the 'force drop' phenomenon, which traditionally leads to erroneous identification of nonlinear structures [40]. However, in certain applications, the force may be altered deliberately to maximise the excitation level but limit local accelerations within their load envelopes to avoid the over-testing of equipment, instruments or subsystems, such as in the force notching test used for ground vibration test campaign in the aerospace industry [27,29,41].

We now demonstrate that the proposed model updating strategy can be applied to cases when the forcing amplitudes vary over a frequency range. A 'simulated' force notching scenario is investigated by taking part of the 1N response data (from 10.8Hz to 11.5Hz) and part of 1.5N response data (from 10-10.8Hz and 11.5-13Hz) to form a notched input. Fig. 14 shows the forcing level of this designed force notching test. This reduces the maximum displacement at location a_2 to less than 6×10^{-3}m.

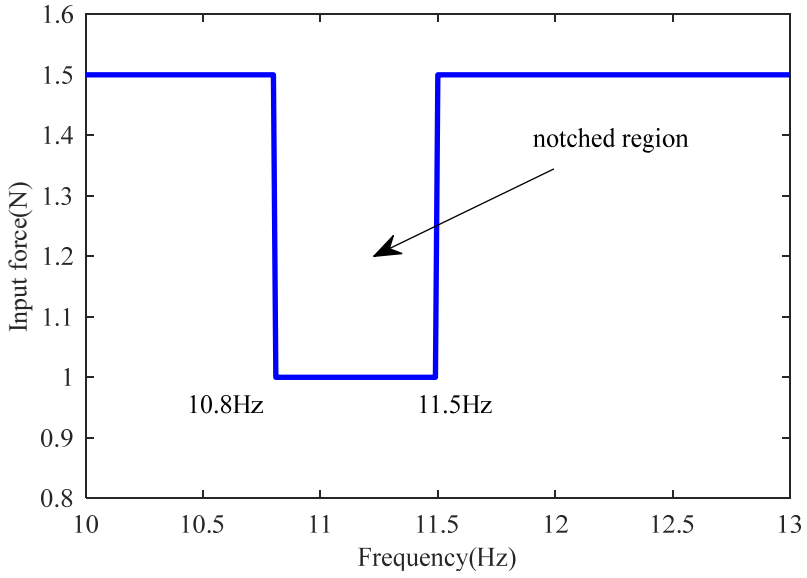

Fig. 14. Input level with intentional notching around the first resonance.

Fig. 15 shows the real Equivalent Dynamic Stiffness plot in the characterisation step using data from the notched input.

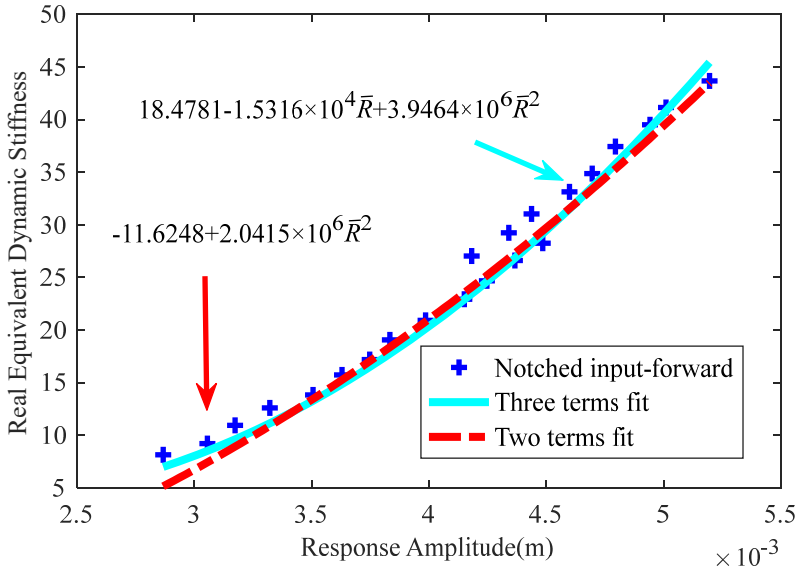

Fig. 15. Real Equivalent Dynamic Stiffness plot with the force notching test: Projection to the $\mathrm{Re}\left(D_{\mathrm{stiff}}\right)-\bar{R}$ plane.

The fitting gives an initial estimation of the nonlinear coefficients as

$$\boldsymbol{\theta}=\left[-11.6248\,\mathrm{N/m},\quad 2.0415\times10^{6}\,\mathrm{N/m^{3}},\quad 12.2393\times10^{-2}\,\mathrm{Ns^{2}/m^{2}}\right]^{\mathrm{T}}. \tag{45}$$

The objective function drops 16.1% with 100 iterations and the parameters converge to

$$\boldsymbol{\theta}=\left[-8.5532\,\mathrm{N/m},\quad 1.9247\times10^{6}\,\mathrm{N/m^{3}},\quad 8.4756\times10^{-2}\,\mathrm{Ns^{2}/m^{2}}\right]^{\mathrm{T}}. \tag{46}$$

Figure 16 compares the measured data with the analytical responses of the updated nonlinear FE model for the notched input, and it can be seen that there is a good agreement between the two.

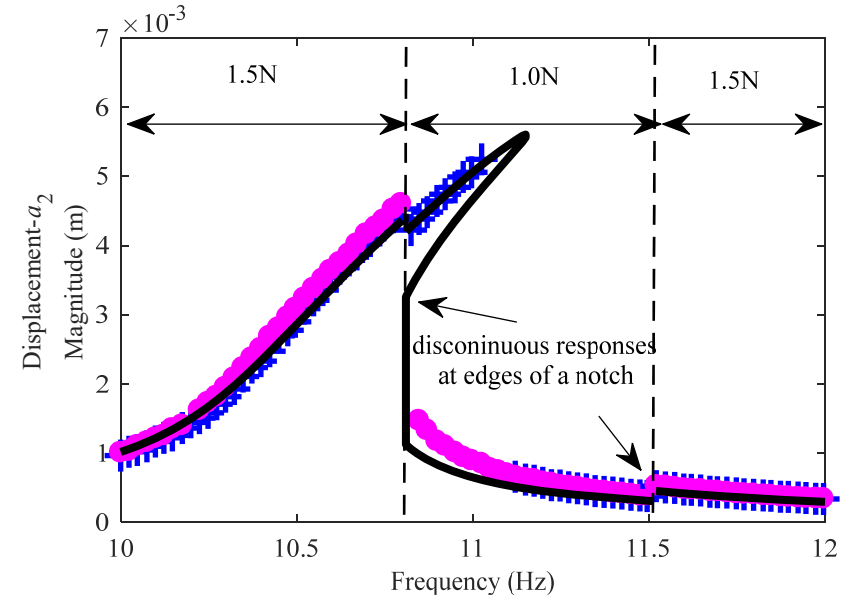

(a)

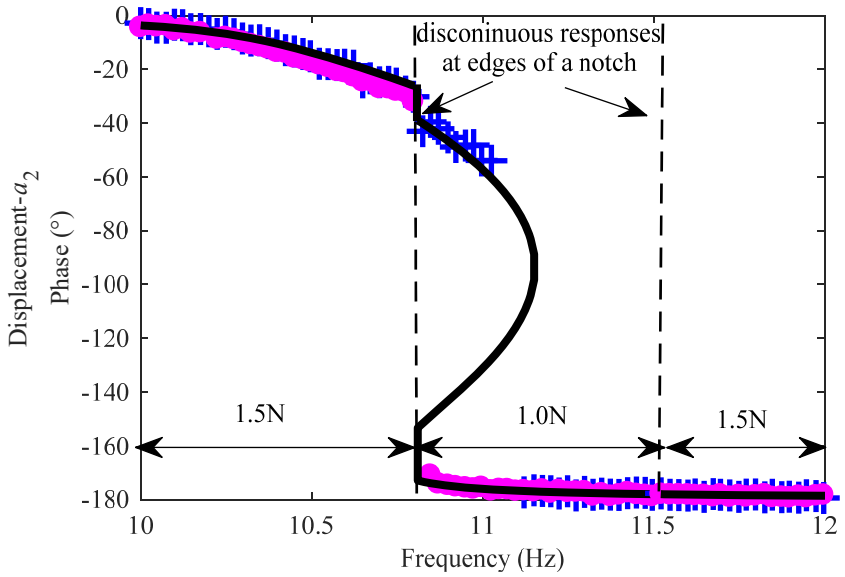

(b)

Fig. 16. Comparison between the measured data and the analytical responses of the updated nonlinear FE model for a force notching test at location a_2. The two plots show (a) magnitude and (b) phase, where (+) and (●) denote the measured data for the notched forward and backward sweeps, respectively, and black line denotes the analytical responses.

5. Conclusions

This paper presents a novel model updating strategy for structures with localised nonlinearities. It starts with an initial FE model of the structure and updates its underlying linear part according to low-amplitude testing results using mature linear model updating theory to reduce the linear errors. Then, it correlates the updated underlying linear FE model with measured primary harmonic frequency response data under high-amplitude stepped-sine and/or slow swept-sine excitations, where the nonlinear distortions are utilised to localise, characterise, and quantify the discrete nonlinear elements. The process is finally validated by comparing the measured and analytically predicted responses at input levels that are not included in the updating. The strategy is demonstrated using experimental data from a clamped beam with a nonlinear mechanism near the tip, and a good agreement between the measured data and the updated model predictions is achieved. Further discussions include the damping estimation and the performance of dealing with amplitude-varying force input.

One advantage, as well as the main motivation of this strategy, is that it relies on data acquired using sinusoidal excitation, an established testing procedure in the aerospace industry. Specifically, the stepped-sine or slow swept-sine excitations are able to drive large-scale structures to close to their in-service energy levels, and generate high-quality and highly reliable data to update the FE model. In addition, amplitude-varying force input data can also be used for this nonlinear model updating strategy. A key advantage of the strategy is that the refined parameter estimation process is based on a novel semi-analytical output residual, which avoids solving the nonlinear dynamic equation to compute analytical responses, allowing fast updating iterations. A further advantage is that the final updated model can directly produce frequency domain responses without time integration, and thereby the model fidelity can be assessed by outputs.

The current strategy deals with primary harmonic responses, and an extension of the strategy to account for multiple harmonics or quasi-periodic responses requires further work. The extraction of the underlying linear dynamics is challenging for structures with friction or clearance types of nonlinearity and also requires further investigation. Characterisation and quantification of nonlinear and lightly damped elements also remain a challenge.

Acknowledgement

The authors gratefully acknowledge the support provided by the EPSRC; X.W. and A.D.S. are supported by the Engineering Nonlinearity programme grant EP/K003836/1 and S.A.N. by fellowship EP/K005375/1. H.H.K. acknowledge the support provided by the EPSRC EP/P01271X/1.

References

1. Friswell M, Mottershead J E. Finite element model updating in structural dynamics [M]. Springer Science & Business Media, 1995.
2. Mottershead J E, Link M, Friswell M I. The sensitivity method in finite element model updating: a tutorial[J]. Mechanical systems and signal processing, 2011, 25(7): 2275-2296.
3. Carney, K., Yunis, I., Smith, K., & Peng, C. Y. Nonlinear dynamic behavior in the Cassini spacecraft modal survey[C]//Proceedings-SPIE The International Society for Optical Engineering. SPIE International Society for Optical, 1997: 811-817.
4. Kerschen, G., Soula, L., Vergniaud, J. B., & Newerla, A. Assessment of nonlinear system identification methods using the smallSat spacecraft structure[M]//Advanced Aerospace Applications, Volume 1. Springer New York, 2011: 203-219.
5. Noël J P, Renson L, Kerschen G. Complex dynamics of a nonlinear aerospace structure: experimental

identification and modal interactions[J]. Journal of Sound and Vibration, 2014, 333(12): 2588-2607.

6. Renson L, Noël J P, Kerschen G. Complex dynamics of a nonlinear aerospace structure: numerical continuation and normal modes[J]. Nonlinear Dynamics, 2015, 79(2): 1293-1309.
7. Göge, D., Sinapius, M., Füllekrug, U., & Link, M. Detection and description of non-linear phenomena in experimental modal analysis via linearity plots[J]. International Journal of Non-Linear Mechanics, 2005, 40(1): 27-48.
8. Bowald M, Link M. Identification of non-linear joint parameters by using frequency response residuals[C]//Proceedings of the 2004 International Conference on Noise and Vibration Engineering (ISMA2004), Leuven, Belgium, September. 2004: 20-22.
9. Noël, J. P., Renson, L., Kerschen, G., Peeters, B., Manzato, S., & Debille, J. Nonlinear dynamic analysis of an F-16 aircraft using GVT data[C]//Proceedings of the international forum on aeroelasticity and structural dynamics. 2013.
10. Dossogne, T., Noël, J. P., Grappasonni, C., Kerschen, G., Peeters, B., Debille, J., Vaes M., & Schoukens, J. Nonlinear ground vibration identification of an F-16 aircraft-Part 2: Understanding Nonlinear Behaviour in Aerospace Structures Using Sine-sweep Testing[C]//Proceedings of the International Forum on Aeroelasticity and Structural Dynamics. 2015.
11. Lee, Y., Vakakis, A., Bergman, L., McFarland, D. M., & Kerschen, G. Suppression aeroelastic instability using broadband passive targeted energy transfers, part 1: Theory[J]. AIAA journal, 2007, 45(3): 693-711.
12. Lee, Y. S., Kerschen, G., McFarland, D. M., Hill, W. J., Nichkawde, C., Strganac, T. W., Bergman, L., & Vakakis, A. F. Suppressing aeroelastic instability using broadband passive targeted energy transfers, part 2: experiments[J]. AIAA journal, 2007, 45(10): 2391-2400.

13. Castrichini, A., Hodigere Siddaramaiah, V., Calderon, D. E., Cooper, J. E., Wilson, T., & Lemmens, Y. Nonlinear Folding Wing Tips for Gust Loads Alleviation[J]. Journal of Aircraft, 2016.

14. Wang Xing, Yao Hongxiang, Zheng Gangtie. Enhancing the isolation performance by a nonlinear secondary spring in the Zener model[J]. Nonlinear dynamics, doi:10.1007/s11071-016-3205-3

15. Wei F, Liang L, Zheng G T. Parametric study for dynamics of spacecraft with local nonlinearities[J]. AIAA journal, 2010, 48(8): 1700-1707.

16. Kerschen G. On the model validation in non-linear structural dynamics[J]. These de doctorat université de Liege, 2002.

17. Kerschen G, Lenaerts V, Golinval J C. Identification of a continuous structure with a geometrical non-linearity. Part I: Conditioned reverse path method[J]. Journal of Sound and Vibration, 2003, 262(4): 889-906.

18. Kerschen, G., Worden, K., Vakakis, A. F., & Golinval, J. C. Past, present and future of nonlinear system identification in structural dynamics[J]. Mechanical systems and signal processing, 2006, 20(3): 505-592.

19. Noël J P, Kerschen G. Nonlinear system identification in structural dynamics: 10 more years of progress[J]. Mechanical Systems and Signal Processing, 2017, 83: 2-35.

20. Ewins D J, Weekes B, delli Carri A. Modal testing for model validation of structures with discrete nonlinearities[J]. Phil. Trans. R. Soc. A, 2015, 373(2051): 20140410.

21. Delli Carri, A., Weekes, B., Di Maio, D., & Ewins, D. J. Extending modal testing technology for model validation of engineering structures with sparse nonlinearities: A first case study[J]. Mechanical Systems and Signal Processing, 2016.

22. Richards C M, Singh R. Identification of multi-degree-of-freedom non-linear systems under random excitations by the “reverse path” spectral method[J]. Journal of Sound and Vibration, 1998, 213(4): 673-708.

23. Vakakis, A. F., L. A. Bergman, D. M. McFarland, Y. S. Lee, and M. Kurt. Current efforts towards a non-linear system identification methodology of broad applicability. Proceedings of the Institution of Mechanical Engineers, Part C: Journal of Mechanical Engineering Science 225, no. 11 (2011): 2497-2515.

24. Kurt M, Eriten M, McFarland D M, et al. Bergman, L. A., & Vakakis, A. F. Methodology for model updating of mechanical components with local nonlinearities[J]. Journal of Sound and Vibration, 2015, 357: 331-348.

25. Peter S, Grundler, A., Reuss, P., Gaul, L., & Leine, R. I. Towards finite element model updating based on nonlinear normal modes[M]//Nonlinear Dynamics, Volume 1. Springer International Publishing, 2016: 209-217.

26. Kurt M, Moore, K. J., Eriten, M., McFarland, D. M., Bergman, L. A., & Vakakis, A. F. Nonlinear model updating applied to the IMAC XXXII Round Robin benchmark system[J]. Mechanical Systems and Signal Processing, 2017, 88: 111-122.

27. A. Calvi, N. Roy, Spacecraft mechanical loads analysis handbook. ESA Requirements and Standards Division, Noordwijk , The Netherlands, 2013.

28. Göge, D., Böswald, M., Füllekrug, U., & Lubrina, P. Ground vibration testing of large aircraft—state-of-the-art and future perspectives[C]//Proceedings of the International Modal Analysis Conference, Orlando. Vol. 1. No. 1. 2007.

29. Lubrina, P., Giclais, S., Stephan, C., Boeswald, M., Govers, Y., & Botargues, N. AIRBUS A350 XWB GVT: State-of-the-art techniques to perform a faster and better GVT campaign[M]//Topics in Modal Analysis II, Volume 8. Springer International Publishing, 2014: 243-256.

30. Tanrikulu, O., Kuran, B., Ozguven, H. N., & Imregun, M. Forced harmonic response analysis of nonlinear structures using describing functions[J]. AIAA journal, 1993, 31(7): 1313-1320.

31. Lin R M. Identification of the dynamic characteristics of nonlinear structures. University of London, 1990.

32. Siller H R E. Non-linear modal analysis methods for engineering structures. University of London, 2004.

33. Canbaloglu, G. and Ozguven, H. N., Model updating of nonlinear structures from measured FRFs, Mechanical Systems and Signal Processing, 2016, 80: 282-301.

34. Wang X., H. Haddad Khodaparastb, A. D. Shaw, M. I. Friswell, Zheng G.T. Localization of local nonlinearities in structural dynamics using spatially incomplete measured data. Mechanical Systems and Signal Processing, 2018, 99: 364-383.

35. Shaw, A. D., Hill, T. L., Neild, S. A., & Friswell, M. I. Periodic responses of a structure with 3: 1 internal resonance[J]. Mechanical Systems and Signal Processing, 2016, 81: 19-34.

36. Noël, J. P., Kerschen, G., Foltête, E., & Cogan, S. Grey-box identification of a non-linear solar array structure using cubic splines[J]. International Journal of Non-Linear Mechanics, 2014, 67: 106-119.

37. Hill, T. L., Green, P. L., Cammarano, A., & Neild, S. A. Fast Bayesian identification of a class of elastic weakly nonlinear systems using backbone curves[J]. Journal of Sound and Vibration, 2016, 360: 156-170.

38. Wang X, Zheng G T. Equivalent Dynamic Stiffness Mapping technique for identifying nonlinear structural elements from frequency response functions[J]. Mechanical Systems and Signal Processing, 2016, 68: 394-415.

39. Ewins, David J. Modal testing: theory and practice. Vol. 15. Letchworth: Research studies press, 1984.

40. Gondhalekar A C. Strategies for non-linear system identification. Imperial College London, 2009.

41. T.D. Scharton. Force Limited Vibration Testing Monograph[R]. NASA Reference Publication RP-1403, May 1997.